A procedure to calculate sound induced vibration using acoustical reciprocity

Keunen, H.

Award date:
2002

A procedure to calculate sound induced vibration using acoustical reciprocity

Master's Thesis

Ing. Harm Keunen

DCT Report nr. 2002-32

June 12, 2002

p. 21

Examination date	June 25, 2002
Committee	Prof.dr. H. Nijmeijer Prof.dr.ir. J.W. Verheij Dr.ir. A de Kraker Dr.ir. G. Verbeek (Paragon Numerical Engineering) Ir. C.A.L. de Hoon (ASML)
Professor	Prof.dr.ir. J.W. Verheij
Coaches	Dr.ir. G. Verbeek (TUE, Paragon Numerical Engineering) Ir. C.A.L. de Hoon (ASML)

Eindhoven University of Technology
Department of Mechanical Engineering
Section of Dynamics and Control Technology

VOORWOORD

Dit project is een afronding van mijn studie aan de Technische Universiteit van Eindhoven. Ik heb in dit project kennis gemaakt met de wereld van de akoestiek en het lijkt erop dat ik daar nog een tijd in zal verblijven.

Zonder de steun van mijn begeleiders Corné de Hoon bij ASML en Bert Verbeek bij de TU/e had ik dit project niet kunnen volbrengen. Daarnaast heeft Professor Jan Verheij mij vaak aan het denken (twijfelen) gezet, over principes uit de akoestiek die toch weer een andere manier van denken vergen. Ik heb door dit project weer heel veel bijgeleerd, wat zeker een van de doelen was toen ik eraan begon.

Met het afronden van dit project rond ik een schoolperiode van 23 jaar af, van kleuterschool tot Universiteit met de basisschool, MAVO, MTS en HTS als tussenstappen. In al die jaren ben ik ondersteund door mijn ouders die ik dan ook heel dankbaar ben voor hun eindeloze support.

Speciaal wil ik mijn vrouw bedanken die mij ook al die jaren heeft gesteund, al was het niet altijd even makkelijk. Mijn laptop gaat nu in de kast.....

Verder wil ik natuurlijk een ieder bedanken die in meer of mindere zin heeft bijgedragen aan het volbrengen van mijn studie en dit project, waaronder de VKO-ers en de DCT-ers.

Deurne, Mei 2002

ABSTRACT

The study described in this report was performed at ASML in Veldhoven in association with the University of Technology in Eindhoven. The objective is to derive a procedure to calculate sound induced vibration of a box shaped model using acoustical reciprocity.

During the development of scanners (machines used for the fabrication of semi-conductors), a lot of computer simulations are done at ASML in order to develop a machine that meets the criteria with respect to dynamical behavior. One of the sources of dynamical disturbance of the metro frame (an important frame in the scanner) is sound induced vibration.

To be able to predict the influence of sound on the metro frame it is necessary to perform sound induced vibration calculations. In the preceding literature study ([Keunen, 2001]) it was found that to be able to perform sound induced vibration calculations a new procedure must be developed as no direct tools were available. It was also found that a box construction like in Figure 1 is dynamically and geometrically rather similar to the construction of the metro frame up to 300 Hz. As the metro frame is a too complex structure to analyze in this project, the box shaped model is used.

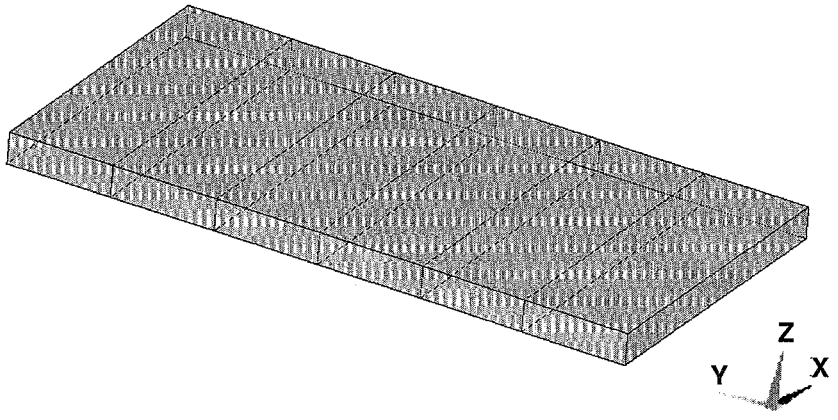

Figure 1 Box construction.

The procedure developed in this project consists of 2 major steps. The first step consists of a mechanical and acoustical calculation to derive a transfer function. It is the transfer function of a force on 1 point (point A) on the box to the radiated sound power of the box. The second step uses this transfer function together with a reciprocity relation to calculate the accelerations on the same point (point A) of the box. The procedure as used in this project only works under the assumption of a diffuse sound field surrounding the box.

As expected, the largest part of the acceleration was due to vibrations at the resonance frequencies. Therefore the contribution of 3 global modeshapes to the total acceleration was predicted up to 200 Hz, a bending mode, a double bending mode and a torsion mode.

To validate the procedure, the predictions were compared to measurements performed prior to this project. The accuracy of the predictions differed through the eigenmodes. The contribution of the bending mode was predicted around a factor 2 times the measurements and the contribution of the double bending mode was predicted within a factor 1.7. No conclusions were drawn from the torsion mode as it was predicted poorly because only a few calculation results were available.

Overall, the procedure developed in this project can predict the accelerations on the surface of a box shaped model up to 200 Hz (induced by a diffuse sound field) within a factor 2.

CONTENTS

NOMENCLATURE

Symbols

a	m/s^2	Acceleration
A	m^2	Equivalent absorbing surface of a room
c	m/s	Speed of sound
F	N	Force
H^2_{tF}	W/N^2	Transfer function due to an excitation force
M	Nm	Torque
p	N/m^2	Sound pressure
p_{rev}	N/m^2	Sound pressure in a reverberant room
P_{rad}	Nm/s	Radiated sound power
ρ	kg/m^3	Density
T_{60}	s	Reverberation time
φ	rad/s	Angular velocity
v	m/s	Velocity
V	m^3/s	Volume velocity
$\dot{V}$	m^3/s^2	Volume acceleration

Notation

$\overline{X}$	Spatial average of variable X
$\vec{x}$	Field information of variable x

CHAPTER 1

INTRODUCTION

The study described in this report was performed at ASML in Veldhoven and at the University of Technology in Eindhoven. It deals with a numerical procedure to analyze sound induced vibration of a box shaped model using structural-acoustical reciprocity.

In this chapter an overview of this project and the function of the metro frame are given. Furthermore the problem definition is given as well as the outline of this report.

1.1 OVERVIEW

ASML is a company that develops, produces, sells and services advanced photolithographic Wafer steppers and Step & Scan systems. These systems are used worldwide for the fabrication of semi-conductors (IC's) for instance at TSMC, AMD, Philips, Samsung and Hyundai.

The scanner is composed of a number of frames (see Figure 2) that give the scanner its stiffness. They form a means to decouple the sensitive parts (clean world, nanometer level) from surrounding less sensitive parts (dirty world, micrometer level).

During the development of a new scanner, a lot of computer simulations are performed in order to develop a machine that meets the criteria with respect to its dynamical behavior. For this purpose a modeling strategy and a system model have been developed. Amongst other things the system model is used for calculating imaging errors. For dynamics these imaging errors are divided in a low frequency part, called overlay (errors), and a high frequency part, called fading (errors).

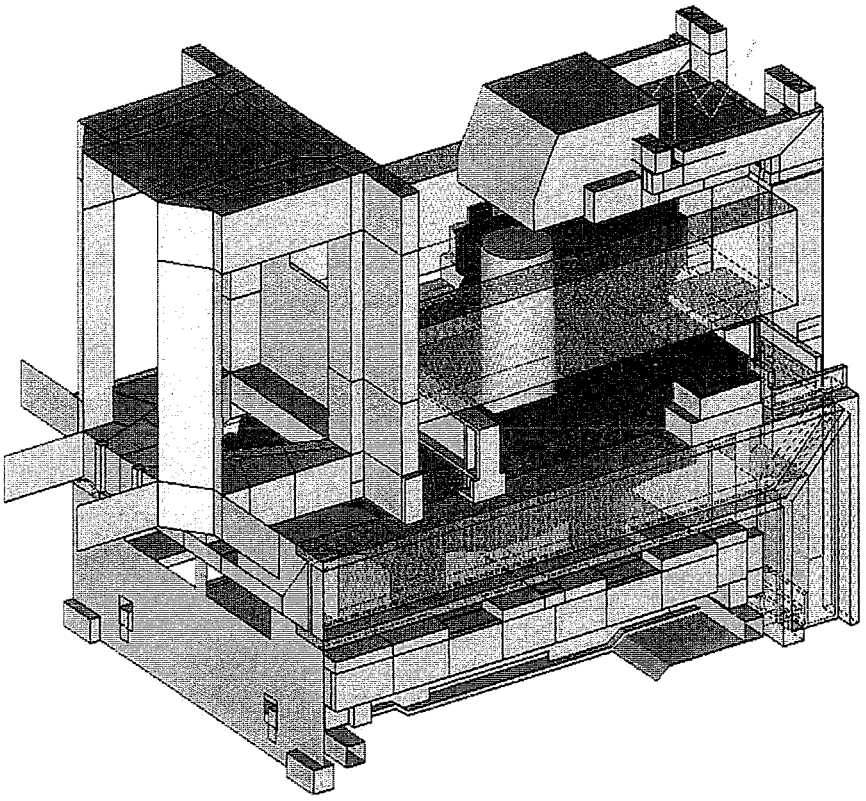

Figure 2 FE model of the scanner assembly.

1.2 THE METRO FRAME

An important frame of the scanner is the metro frame (red in Figure 2), which holds the lens (yellow in Figure 2) and part of the metrological equipment. It is typically a frame in the clean world, which means that the allowed vibration level is rather low (nanometers). Physical decoupling between the base frame (gray in Figure 2) and the metro frame is done by means of airmounts. These airmounts isolate the metro frame from base frame vibrations for frequencies above 0.5 Hz.

One of the remaining sources of dynamical disturbances of the metro frame is sound induced vibration. Two major causes are responsible for this acoustical excitation. One is the clean air system [TNO, 2000], the other is the environmental sound pressure level generated outside the exposure unit due to adjacent steppers, scanners, tracks and "normal" sounds in the clean room [Gompel, 2000].

At the beginning of this project, some research was available already. To perform research on the acoustical sensitivity of the metro frame, at ASML a simplified physical model has been made. This physical model, a closed box, was experimentally investigated in a reverberant room. Moreover numerical studies have been performed, creating Matlab and Sysnoise models of the box to predict surface accelerations due to sound excitation. The measurements along with the numerical studies are useful to gain insight in sound induced vibration, [Hoon, 2000].

1.3 PROBLEM DEFINITION

For next generation scanners using extreme ultraviolet light (EUV), sound induced vibrations will be less of a problem, as the most important parts of the system will function in a vacuum. However for the near future scanners, with tightened specifications, sound is an important excitation force. To be able to predict the influence of sound on parts of the scanner it is necessary to make sound induced vibration calculations. In the preceding literature study ([Keunen, 2001]) it was found that to be able to make sound induced vibration calculations, a new procedure needed to be developed as no appropriate tools were available.

At Paragon Numerical Engineering, a new sound radiation program has been created, NEO, which uses the boundary elements method (BEM, see [NEO, 2001]). As it is not possible to perform sound induced vibration calculations with NEO directly, an indirect way must be found.

A reciprocity relation exists which links sound radiation due to mechanical excitation to sound induced vibration. NEO in combination with the reciprocity relation can be used in a calculation of sound induced vibration.

Measurements have been performed on a closed box, resembling the metro frame; the model in this project will therefore also be a closed box. This makes it possible to use the measurements for validating the calculations. The metroframe is a too complex structure to use at this stage.

The objective of this study is to derive a procedure to calculate sound induced vibration of a box shaped model using acoustical reciprocity.

1.4 OUTLINE OF THIS REPORT

After the introduction some background information on the project is given in Chapter 2. It is described how the model was accomplished and some measurement results are given.

In Chapter 3 the procedure is developed to calculate sound induced vibration of a box shaped model using a finite element model, a boundary element model and acoustical reciprocity. At first the theory of acoustical reciprocity is discussed, secondly a way of applying this on a model is presented.

Chapter 4 will show some results of the procedure applied on a box shaped model. Also a validation step is carried out to check the procedure.

The conclusions and recommendations of this project will be presented in Chapter 5.

CHAPTER 2

BACKGROUND INFORMATION

As an analysis of the metro frame is too complex at this stage, a simplified construction is modeled. The global low frequency dynamical behavior (till 180 Hz) of this construction must be reasonably in resemblance with that of the metro frame. A closed box can be considered as a suitable construction to resemble the metro frame. In this chapter the description of the box construction is given as well as some measurement results. These measurements were performed by De Hoon and others and are described in detail in [Hoon, 2000].

2.1 THE BOX CONSTRUCTION

For a box construction, the top and the bottom plates have large areas, making it sensitive to acoustical excitation. To suppress low frequency plate modes, vertical plates are present inside the box connecting the top and bottom plate. These vertical plates hardly influence the bending around the x-axis and the torsion.

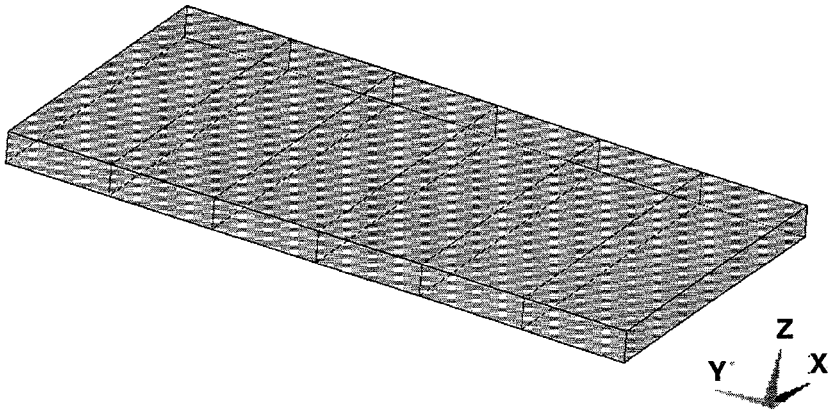

Figure 3 Box construction.

To resemble the global dynamical behavior of the metro frame, the dimensions of the box are 1.0 x 2.0 x 0.1 [m], with 5 vertical plates on the inside (dashed lines in Figure 3). The overall plate thickness is 5 [mm] except for the plates on the short sides, which are 25 [mm] thick. The dimensions were derived from finite element calculations by calculating bending and torsional modes of the frame [Hoon, 2000].

The material of the box is stainless steel; the material properties are shown in Table 1.

Table 1 Material properties of stainless steel.

Material property	Value
Young's modulus	210e9 [N/m^2]
Poisson's ratio	0.33 [-]
Density	7800 [kg/m^3]

To gain insight in the dynamical behavior of the box, measurements have been done on a physical model. Therefore a box was welded by slotweldings of 10 [cm], where the ratio of welded and unwelded length is 50-50 (50% welded and 50% not welded). In pre-studies at ASML it is found that this way of connecting plates should have little influence on the dynamical behavior up to 300 Hz. Most of the frames in the scanners are welded in this way.

As the box is meant to model the metro frame, some assumptions were made before measuring.

2.2 ASSUMPTIONS

The metro frame-lens assembly is built in the scanner surrounded by all kinds of structures, resulting in reflection of sound from all directions. The sound field can therefore not be represented by one or a few point sources, as this will bring directional sensitivity. Sound measurements have shown that the sound pressure levels surrounding the metro frame are roughly constant. Under these circumstances the sound field around the metro frame is assumed to be diffuse (see Appendix A for the characteristic properties of a diffuse field).

The metro frame is attached to the scanner by means of airmounts. These airmounts decouple the metro frame from the base frame vibrations. In the following measurements, the box was suspended by three very soft elastic springs, thus determining the virtually free dynamical behavior at audible frequencies. In the calculations of Chapter 4 the box is also assumed free from displacement boundary conditions (no connection to the fixed world).

2.3 MEASUREMENT RESULTS

Various measurements were performed to determine the dynamical behavior of the box till 200 Hz. First the eigenfrequencies and mode shapes were measured. Than the transfer functions were measured to determine the modal damping values. Finally acoustical measurements were executed, making it possible to validate acoustical calculations and to gain insight into the behavior of the box in a diffuse field.

2.3.1 EIGENFREQUENCIES AND MODE SHAPES

The eigenfrequencies and mode shapes have been determined experimentally in order to gain insight into the global dynamical behavior and to be able to verify the FE models. In the experiments the box was suspended by three very soft elastic springs, thus determining the free-free eigenmodes.

With a hammer the box was excited in z-direction (perpendicular to the top plate). Modes that predominantly vibrate in x and y-direction (see Figure 3) have higher frequencies and are not considered relevant. The resulting accelerations were measured at different places on the top of the box. These results were imported in Star version 5.2 (Modal Analysis package), where an advanced auto fitter can calculate mode shapes and eigenfrequencies.

On the surface of the box a lot of local plate deformation patterns (plate modes) are found. However, only the first three global modes will be taken into account, as they are found in the metro frame as well as in the box. For a description of the mode shapes and the according frequencies see Table 2.

Table 2 Modal analysis, measurement results.

Mode shape	Frequency [Hz]
Bending mode around the x-axis	95.9
Double bending mode around the x-axis	139.1
Torsion mode	159.1

2.3.2 DAMPING PROPERTIES

Hanging free in elastic springs, the box was excited by a shaker at a corner point of the box in z-direction. At this point the accelerations were measured, for three modes (bending, double-bending and torsion) separately. In Table 3 the measured modal damping values are shown.

Table 3 Measured modal damping values.

Mode shape	Damping [%]
Bending around the x-axis	0.48
Double bending around the x-axis	0.40
Torsion	0.35

2.3.3 ACOUSTICAL MEASUREMENTS

The acoustical measurements have been performed at Philips Natlab in a reverberant room. This is a room in which volume, shape and wall characteristics are such that the mean sound intensity is independent on the location in the room (except very close to the wall and sound source). It has been checked that the distance between the walls and the box is large enough for having a diffuse field around the box.

Again the box was hanging free in elastic springs and a loud fan (B&K) is used as excitation source, producing a flat sound spectrum of about 90 db. The sound produced by the source at about 2.5 [m] from the box will induce vibration of the box.

On the box the z-acceleration was measured at different locations. 6 of these locations that will be calculated later on in Chapter 4 are shown in Figure 4. The results of the acceleration measurements are shown and used in the validation step of paragraph 4.4.

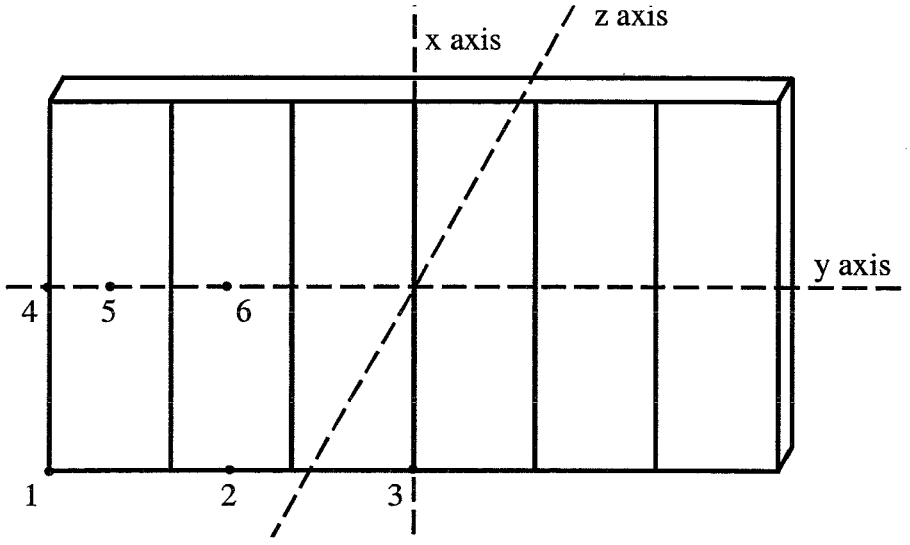

Figure 4 Locations where the z-accelerations were measured.

As mentioned before, a procedure must be developed to perform sound induced vibration calculations with the use of acoustical reciprocity. In the next chapter, acoustical reciprocity will be discussed and applied to the box.

CHAPTER 3

ACOUSTICAL RECIPROCITY

At the start of this project no tools were available for direct sound induced vibration calculations. There is however software (NEO) available at the University of Technology in Eindhoven, which uses the boundary elements method (BEM) for calculation of sound radiation. Moreover, an acoustical reciprocity relation can be exploited which links sound radiation due to a mechanical excitation to sound induced vibration. Combining NEO with this reciprocity relation results in a procedure to calculate sound induced vibration.

In this chapter the theory of acoustical reciprocity will be discussed, as well as a way of applying this theory on a model for sound induced vibration.

3.1 THEORY

In the field of structural acoustics there are already applications of reciprocity, mostly in experimental methods. In ship acoustics for instance reciprocity can be used for analyzing transmission paths that contribute to sound radiation into the water. Replacing the inboard mechanical excitations by an outboard acoustical excitation with an underwater sound source has a number of potential experimental advantages. These include a better signal-to-noise ratio, no space problems for exciters and no difficult excitations such as torques or in-plane forces.

Loosely speaking, the principle of reciprocity states that the response of a linear system to a disturbance which is applied at some point by an external agent, is unchanged if the points of input and observed response are reversed [Fahy, 1990].

Hereafter, the principle of reciprocity is introduced in 3 steps. Step 1 considers reciprocity in a mechanical system, step 2 in an acoustical system and step 3 combines the two in a mechanical-acoustical system (see [Verheij, 1994] and [Verheij, 1996]).

3.1.1 MECHANICAL SYSTEM

The simplest representation of a network composed of linear, passive mechanical elements is a 2-port system as given in Figure 5. Each port corresponds with a single physical point and a single vibrational degree of freedom. When the system is vibrating about a configuration of stable equilibrium this system is reciprocal.

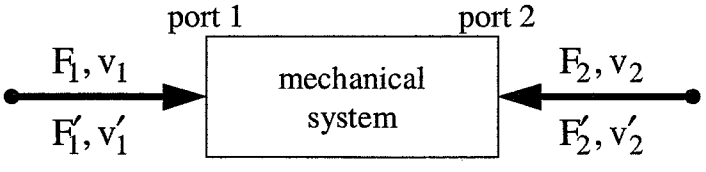

Figure 5 Mechanical 2-port system.

At the two ports the conjugate variable pairs F_1, v_1 and F_2, v_2 denote complex phasors (conjugate means that the time averaged product equals the mean power flow); harmonic signals are assumed. The sign convention is chosen in such a way that a positive energy flow is directed inwards. Through successive excitation at port 1 and port2, two different sets of forces and velocities are considered (F_1, v_1, F_2, v_2 and F_1', v_1', F_2', v_2'). The basic reciprocity theorem says:

Equation 1 $$F_1' v_1 + F_2' v_2 = F_1 v_1' + F_2 v_2'$$

From the reciprocity theorem (Equation 1) and various boundary conditions three special reciprocity relations can be developed (Equation 2).

Equation 2 $$H = \left.\frac{v_2}{F_1}\right|_{F_2=0} = \left.\frac{v_1'}{F_2'}\right|_{F_1'=0}, \quad H = \left.\frac{F_2}{v_1}\right|_{v_2=0} = \left.\frac{F_1'}{v_2'}\right|_{v_1'=0} \quad \text{and} \quad H = \left.\frac{F_2}{F_1}\right|_{v_2=0} = -\left.\frac{v_1'}{v_2'}\right|_{F_1'=0}$$

The advantage of these special reciprocity relations is that the corresponding transfer functions (H) can be measured in two ways. Take for instance the first relation of Equation 2; by driving the system at port 1; H is measured "directly" $H = \frac{v_2}{F_1}$. By driving the system at port 2; H is measured "reciprocally" $H = \frac{v_1'}{F_2'}$.

Expanding the reciprocity theorem from a 2-port to an n-port system results in Equation 3.

Equation 3 $$\sum_{j=1}^{n} F_j' v_j = \sum_{j=1}^{n} F_j v_j'$$

This expansion makes it for instance possible to define 6 degrees of freedom (DOF) per spatial point, resulting in a 12 port system (F_{1x}, v_{1x}; F_{1y}, v_{1y}; F_{1z}, v_{1z}; M_{1x}, φ_{1x}; M_{1y}, φ_{1y}; M_{1z}, φ_{1z}; F_{2x}, v_{2x}; ..... ; M_{2z}, φ_{2z};). An example of a special reciprocity relation of the 12-port system is given in Equation 4.

Equation 4 $$H = \left.\frac{v_{2x}}{F_{1y}}\right|_{\substack{\text{Other} \\ 11\ F=0}} = \left.\frac{v_{1y}'}{F_{2x}'}\right|_{\substack{\text{Other} \\ 11\ F'=0}}$$

Now the transfer function of the mechanical two-port multiple DOF system is derived, next the acoustical system is analyzed.

3.1.2 ACOUSTICAL SYSTEM

Passive, linear acoustical systems that vibrate about a configuration of stable equilibrium are reciprocal. The reciprocity theorems and the reciprocity relations are quite similar to those of mechanical systems. The conjugate variable pairs of pressures and volume velocities are p_1, V_1 and p_2, V_2. The reciprocity theorem analogous to Equation 1 is:

Equation 5 $$p_1' V_1 + p_2' V_2 = p_1 V_1' + p_2 V_2'$$

Special reciprocity relations equivalent to Equation 2 are:

Equation 6

$$\left.\frac{p_2}{V_1}\right|_{V_2=0} = \left.\frac{p_1'}{V_2'}\right|_{V_1'=0} \quad , \quad \left.\frac{V_2}{p_1}\right|_{p_2=0} = \left.\frac{V_1'}{p_2'}\right|_{p_1'=0} \quad \text{and} \quad \left.\frac{p_2}{p_1}\right|_{V_2=0} = -\left.\frac{V_1'}{V_2'}\right|_{p_1'=0}$$

In Equation 6 the boundary condition $V_x=0$ is prescribed. This is in practice not exactly met, but measurements with a pressure microphone which has a large acoustical impedance do approximate this well.

The simplest sources and receivers for which Equation 6 is valid are point monopole sources and receivers. Higher order sources and receivers (dipole a.o.) can be modeled as a linear combination of monopole sources and receivers (similar to Equation 3).

Now that the mechanical two-port multiple DOF system and the acoustical two-port single DOF system are determined, the interconnected system can be worked out.

3.1.3 MECHANICAL-ACOUSTICAL SYSTEM

A heterogeneous n-port system is reciprocal under the same conditions as for the separate systems. The general reciprocity theorem for an n-port, with m structural ports and one acoustical port is a combination of Equation 3 and Equation 5.

Equation 7

$$\sum_{i=1}^{m} F_{1i}' v_{1i} + p_2' V_2 = \sum_{i=1}^{m} F_{1i} v_{1i}' + p_2 V_2'$$

The conjugate variable pairs in case of a 6 DOF mechanical and one DOF acoustical system are: F_{1x}, v_{1x}; F_{1y}, v_{1y}; F_{1z}, v_{1z}; M_{1x}, φ_{1x}; M_{1y}, φ_{1y}; M_{1z}, φ_{1z} and p_2, V_2 (see Figure 6).

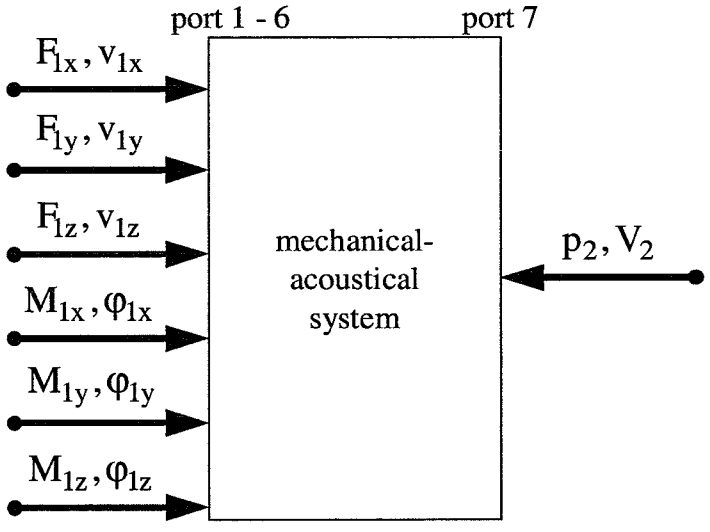

Figure 6 Mechanical-acoustical 7-port system.

One of the special reciprocity relations, which can be derived from Equation 7 with boundary conditions, is as follows;

Equation 8

$$H_{tF} = \left.\frac{p_2}{F_{1z}}\right|_{V_2=0} = -\left.\frac{v_{1z}'}{V_2'}\right|_{\substack{\text{all}F'=0 \\ \text{all}M'=0}}$$

Because sinusoidal time signals have been supposed, it is easy to see that this special reciprocity relation remains valid for time integrated or time differentiated systems. The velocities and volume velocities in Equation 8 can therefore be replaced by the corresponding accelerations (Equation 9).

Equation 9

$$H_{tF} = \frac{p_2}{F_{1z}}\bigg|_{\dot{V}_2=0} = -\frac{a'_{1z}}{\dot{V}'_2}\bigg|_{\substack{\text{all } F'=0 \\ \text{all } M'=0}}$$

Equation 9 is a special reciprocity relation that can be applied as shown in Figure 7.

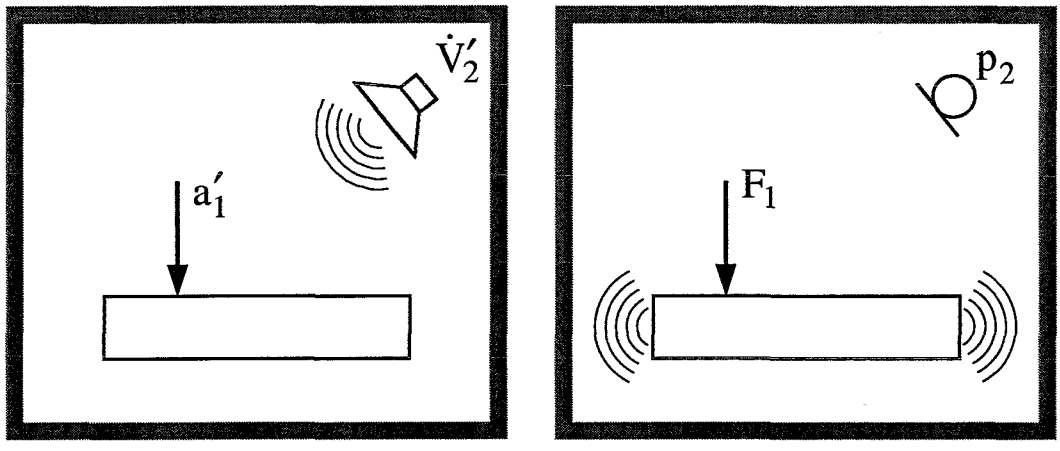

Figure 7 a. Acoustical excitation. b. Mechanical excitation.

In the experiment of Figure 7a, the box is acoustically excited by a sound field. The source is a loudspeaker at point 2 that can be seen as a point monopole source having a volume acceleration $\dot{V}'_2$. As the loudspeaker is located in a reverberant room, the sound field generated will be diffuse (see Appendix A). To determine the transfer function of the box, the accelerations are measured at point 1 on the surface of the box. As seen in Equation 9, the forces and moments on the box must all be zero.

The other way to find the same transfer function of the box can be seen in the experiment of Figure 7b. To determine the transfer function of the box, a force is placed at point 1 to excite the box. The resulting vibrations induce a pressure field that is measured by means of a microphone, at point 2. The microphone can be seen as a point monopole receiver. In Equation 9 it is seen that at point 2 the volume acceleration must be zero, this is accomplished with a high impedance microphone.

The following paragraph will show how to use Equation 9 in a practical example.

3.1.4 EXCITATION OF STRUCTURES

To determine the total sound transfer function of a structural component an equivalent reciprocal experiment is shown in Figure 8.

This transfer function is defined as

Equation 10

$$H^2_{tF} = \frac{P_{rad}}{F_1^2}$$

This is the ratio of the acoustical power P_{rad} radiated by a structural component to the mean square of the excitation force, F_1^2. This transfer function can for instance be used to look for excitation positions with minimum sound radiation (see Figure 8a). In reverse, positions with low vibrations due to acoustical excitation (Figure 8b) are found by using the equivalent reciprocal transfer function Equation 11 (see [Verheij, 1994]).

Equation 11 $$H_{tF}^2 = \frac{\rho}{4 \cdot \pi \cdot c} \cdot \frac{a_1'^2}{\overline{p_{rev}'^2}}$$

where:

a_1' = Acceleration of a point on the structural component in Figure 8b.

$\overline{p_{rev}'^2}$ = Reverberant sound field.

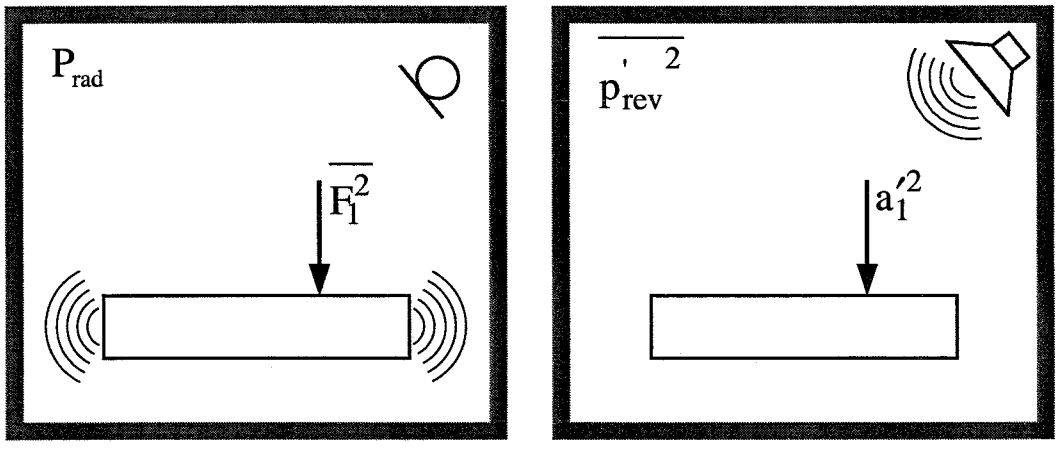

Figure 8 **a.** Sound due to mechanical excitation. ("direct" experiment) **b.** Sound induced vibration. ("reciprocal" experiment)

The point-to-point relation that forms the basis of the "reciprocal" transfer function was given in Equation 9, i.e.

Equation 12 $$\frac{p_2^2}{F_1^2} = \frac{a_1'^2}{\dot{V}_2'^2}$$

where:

p_2 = Pressure measured by a fictitious monopole receiver which is at the microphone position in Figure 8a.

$\dot{V}_2'$ = Volume acceleration of a fictitious monopole source which is at the speaker position in Figure 8b.

Consider experiments for many speaker and microphone positions in the rooms. Now Equation 12 holds for spatial averaging over point receiver and point source positions in the room.

Equation 13 $$\overline{\left[\frac{p_2'^2}{F_1^2}\right]} = \overline{\left[\frac{a_1'^2}{\dot{V}_2'^2}\right]}$$

The assumption of a "diffuse" reverberant sound field gives for the direct experiment

Equation 14
$$\frac{P_{rad}}{F_1^2} = \overline{\left[\frac{p_{rev}^2}{F_1^2}\right]} \cdot \frac{A}{4 \cdot \rho \cdot c}$$

where A denotes the equivalent absorbing surface of the room (see Appendix A).

The sound power generated in the reverberant room by the loudspeaker in the reciprocity experiment (Figure 8b) can according to Appendix A be represented by

Equation 15
$$P'_{rad} = \overline{p'^2_{rev}} \cdot \frac{A}{4 \cdot \rho \cdot c}$$

This field can be imagined to be equal to the room response for excitation with a point source $\dot{V}'_2$ when averaging over source positions. Using the free field radiation resistance of a point monopole source (see [Kinsler, 1982]), one obtains

Equation 16
$$P'_{rad} = \overline{\dot{V}'^2_2} \cdot \frac{\rho}{4 \cdot \pi \cdot c}$$

Substituting Equation 16 into Equation 15 leads to

Equation 17
$$\frac{A}{4 \cdot \rho \cdot c} = \overline{\left[\frac{\dot{V}'^2_2}{p'^2_{rev}}\right]} \cdot \frac{\rho}{4 \cdot \pi \cdot c}$$

Substituting Equation 17 and Equation 13 into Equation 14 leads to a reciprocity relation

Equation 18
$$\frac{P_{rad}}{F_1^2} = \frac{\rho}{4 \cdot \pi \cdot c} \cdot \frac{a'^2_1}{\overline{p'^2_{rev}}}$$

The relation found is usable in different ways, depending on the intended result and the availability of tools and measurements. Considering the objective of this study, Equation 18 can be rewritten as

Equation 19
$$\frac{a'^2_1}{\overline{p'^2_{rev}}} = \frac{P_{rad}}{F_1^2} \cdot \frac{4 \cdot \pi \cdot c}{\rho} = H_{tF}^2 \cdot \frac{4 \cdot \pi \cdot c}{\rho}$$

In order to be able to use this equation for the calculation of sound induced vibrations, a transfer function H_{tF}^2 must be found by means of structural and acoustical calculations. In the following paragraphs the procedure to use Equation 19 will be further explained.

3.2 APPLICATION OF THE PROCEDURE

To use the reciprocity relation of Equation 19 in practice a procedure must be developed as shown in Figure 9. First the surrounding pressure field induced by a force on the surface (point 1) is calculated in two steps, a mechanical and an acoustical step. The reciprocal part can then be executed to calculate the accelerations on the surface (point 1).

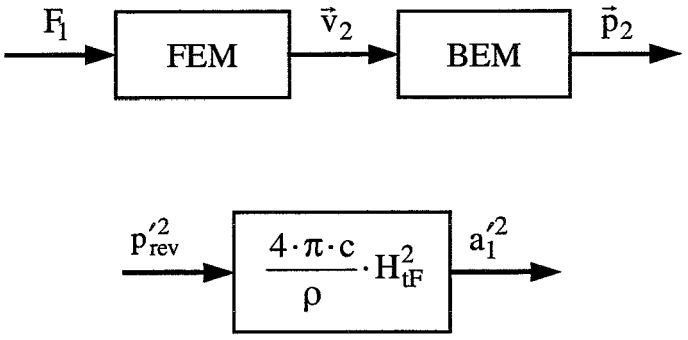

Figure 9 Reciprocity procedure.

3.2.1 MECHANICAL ANALYSIS

The mechanical part of the procedure deals with the structural analysis of the model. As can be seen in Figure 9 the input of the model must be a force at location 1, and the output is a velocity field. To realize this, a FEM (Finite Element Modeling) model is made in ANSYS version 6.0. ANSYS is a FEM package amongst others used for performing various structural calculations.

As discussed in Chapter 2 the model of the metro frame is a welded box construction. The plates of the box are welded together in a 50-50 ratio (50% welded and 50% not welded). This is accounted for in the model by rigidly connecting elements at the locations of the weldings, and not connecting them at the other locations.

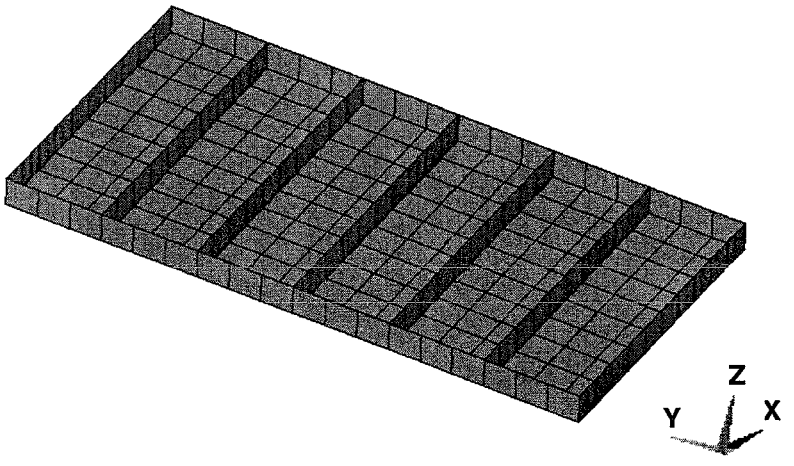

Figure 10 FE model without top plate.

In Figure 10 the FEM mesh is shown, while for presentation convenience the top plate is left out so that the inner plates are visible. The model consisted of higher order shell elements (8 nodes per element, 6 DOF per node) for better bending results. The number of elements was varied through the analyses to try to find the least number of elements with still sufficient accurate results. Between welds there must be at least 2 elements, which raised the number of elements.

The FEM analysis consists of 2 stages: the modal analysis and the harmonic response calculation using modal superposition. In Appendix B these stages are explained in detail. For now it is enough to mention that these analyses result in a frequency dependent nodal velocity field. In practice this FEM step was a problematic and time-consuming one (see notes).

Notes:

In Ansys it is normally possible to define different load cases and solve them successively. In this project however it takes some file handling. The first stage, the modal analysis, is identical in all load cases, as no structural changes are made. Defining and solving different modal superposition analyses based on one modal analysis does not work easily. Naming, renaming and copying database and result files solved this problem.

The frequency steps should be very small to describe the frequency peaks accurately enough, but this increases the calculation time. In ANSYS it is possible to cluster frequency steps around the eigenfrequencies in the mode superposition analysis. This option appears to be useful, but further on in the analysis it causes problems. On the other hand choosing equidistant small frequency steps is not an option, as this will raise the number of calculation steps enormously when the frequency range is increased (especially in the acoustical calculation). In the future, there should be a smart way of picking a number of frequency steps to export to NEO.

These two problems (load cases and frequency clustering) are usually overcome by using Matlab. After the modal analysis it is possible to export the mode shapes and eigenfrequencies from Ansys to Matlab to solve the modal superposition analysis. In Matlab it is easier to manipulate with matrices for the definition of load cases or a frequency range. In this project however, this is not an option, as all nodes on the surface must be taken into account, resulting in even for Matlab computational matrices. In Ansys there are dedicated solvers to solve these large matrices.

Furthermore it is very important to define all element normals outwards because they are used in the acoustical part to define the direction of the boundary conditions.

The steps taken to solve the mechanical part of the procedure were:

- Pre-processor in ANSYS:
  - Define the structural model, that is, the elements and nodes and the element type.
  - Define the material properties of the structure.
- Solver in ANSYS:
  - Solve the modal analysis.
  - Define the boundary condition, that is, one nodal force per load case.
  - Define the modal damping.
  - Define the frequency range and the number of frequency steps.
  - Solve mode superposition analysis per load case.
  - Expand the mode superposition results to create nodal velocity results per load case.

- Post-processor in ANSYS:
    - Select the outer surface of the FE model.
    - Export the nodes and elements from the FE model to ASCII file 1.
    - Export real and imaginary parts of the nodal velocity fields per frequency calculated in the structural step to ASCII file 2.

Now that the structural results have been calculated, these results form the boundary conditions for the acoustical part.

3.2.2 ACOUSTICAL ANALYSIS

The acoustical part of the procedure deals with the structure-fluid relations. As can be seen in Figure 9 the input of the model is the nodal velocity field from the FEM analysis and the output is the acoustical power. To realize this, a BEM (Boundary Element Method) model is made in NEO. NEO is a BEM package used for performing acoustical calculations, both for intern and extern acoustical analyses. Typically, the acoustical excitation of the box per surrounding sound is an external acoustical problem.

Some remarks about using BEM are:

- Only linear problems can be solved, because the basis of the BEM formulation is the potential theory (see [BEM] chapter 2 and 10 for more information).
- Mesh dimensionality is one dimension lower than in FEM (if the FEM mesh is 3d then the BEM mesh is 2d), because only the interfaces between the surrounding fluid and the constructions are meshed.
- Full complex matrices need to be solved at all frequency steps. Thus using the same mesh as the FEM mesh results in large calculation times.

Notes:

In NEO it is not possible to generate a box-like mesh (only a sphere can be build). If it would be possible, the numbering should be exactly the same as in the FE model. This is because the velocity field generated by the FEM calculations must be defined as complex velocity amplitudes on nodes. To be able to build the box-shaped model, nodes and elements from the FE model must be exported to the BEM package.

As mentioned before, in contrast with FEM, only a coarse 2D mesh, lying on the outer surface of the construction must be generated in BEM. Therefore, only elements on the outer surface of the FEM mesh must be selected before exporting to BEM. It must be mentioned that if the complexity of the model rises, it will be harder (more time-consuming) to select the right elements.

In BEM a coarser mesh should be created to lower the calculation times. But, as the resulting nodal velocity field from FEM is the boundary condition for the BE model there should be an interpolation step to be able to coarsen the mesh. In NEO there is no interpolation possibility, therefore it is chosen to use the exact FE model in the BEM analysis. This is not optimal, but for the moment the best solution.

As the BE model and the boundary conditions (velocity fields) are defined, the fluid properties must be given (see Table 4).

Table 4 Fluid properties of air.

Fluid property	Value
Sound speed	343 [m/s]
Density	1.2 [kg/m^3]

The pressures and velocities in the fluid are determined in NEO by solving the Kirchhoff-Helmholtz integral (see [Fahy, 1985] page 115). They are used for calculating the resulting radiated sound power (see [Verheij, 1996] page 2-010).

The steps taken to solve the acoustical part of the procedure were:

- In NEO:
  - Import the nodes and elements from ASCII file 1.
  - Import the resulting velocity fields from ASCII file 2 and use it as boundary conditions for the BE model. These boundary conditions are imported per frequency step so as a consequence; the frequencies to calculate the power results are defined accordingly.
  - Define the surrounding fluid properties.
  - Solve the acoustical problem, resulting in the radiated sound power.

Having determined the radiated sound power and the input force, a transfer function H_{tF}^2 must be calculated.

3.2.3 TRANSFER FUNCTION

With the sound power derived from the BEM analysis and the input force from the FEM analysis, the transfer function (Equation 10) of the structure can be calculated. It is the transfer function of one point to the radiated sound power as seen in Equation 20.

Equation 20 $$H_{tF}^2 = \frac{P_{rad}}{F_1^2}\left[\frac{W}{N^2}\right]$$

The transfer function is used to calculate surface accelerations by means of the reciprocity theory.

3.2.4 RECIPROCAL ANALYSIS

The reciprocal part of the procedure deals with the last step of the procedure where the numerical information comes together. To realize this step, Matlab version 6.0 is used.

Equation 19 in paragraph 3.1.4 shows the reciprocity relation needed. Substituting Equation 20 results in:

Equation 21
$$\frac{P_{rad}}{F^2}\cdot\frac{4\cdot\pi\cdot c}{\rho}=\frac{a_1'^2}{\overline{p_{rev}'^2}} \Rightarrow a_1'^2=\frac{P_{rad}}{F^2}\cdot\overline{p_{rev}'^2}\cdot\frac{4\cdot\pi\cdot c}{\rho}$$

where:

$\overline{p_{rev}'^2}$ = Mean squared sound pressure measured nearby the box; this is a PSD [Pa^2/Hz].

The squared acceleration resulting from Equation 21 will also be in the form of a PSD [(m/s^2)/Hz]. For more information about PSD's see Appendix C. Rewriting Equation 21 with PSD's results in

Equation 22
$$\frac{P_{rad}}{F^2}\cdot\frac{4\cdot\pi\cdot c}{\rho}=\frac{PSD_{out}}{PSD_{in}} \Rightarrow PSD_{out}=PSD_{in}\cdot\frac{P_{rad}}{F^2}\cdot\frac{4\cdot\pi\cdot c}{\rho}$$

The following formula holds for the standard deviation σ that defines the variation of a signal:

Equation 23
$$\sigma=\sqrt{\frac{\sum_{i=1}^{n}(x_i-\overline{x}_n)^2}{n}}$$

The cumulative squared σ is in the case of a PSD defined as:

Equation 24
$$\sigma^2=\sum(PSD_{out}\cdot df)$$

where:

df = Frequency step size.

For a random signal, the cumulative 3σ value is a good measure for the amplitude. The acceleration 3σ value is:

Equation 25
$$3\sigma_{accel}=3\sqrt{\sum(PSD_{out}\cdot df)}$$

For the displacement 3σ value holds:

Equation 26
$$3\sigma_{displ}=3\sqrt{\frac{\sum(PSD_{out}\cdot df)}{(j\omega)^4}}$$

The steps taken to solve the reciprocal part of the procedure are:

- In Matlab:
    - Import the radiated sound power per frequency from a binary NEO file.
    - Import the measured mean sound pressure PSD file.
    - Calculate the cumulative 3σ acceleration or displacement values.

In this chapter, the theory of the reciprocity procedure was explained. In the next chapter the results of the procedure applied to the box will be shown and compared with measurement results.

CHAPTER 4

CALCULATION RESULTS

In this chapter the calculated results of the procedure developed in the previous chapter are shown, after which a comparison between calculations and measurements will be carried out.

4.1 MECHANICAL RESULTS

Because the accelerations at 6 points are wanted, on these points the input forces will be placed. As the reciprocity relation used is a point-to-point relation, 6 different load cases are therefore defined.

The 6 load cases are shown in Figure 11 where the numbers stand for the number of the load case. In all load cases, the force is placed in the same direction (z).

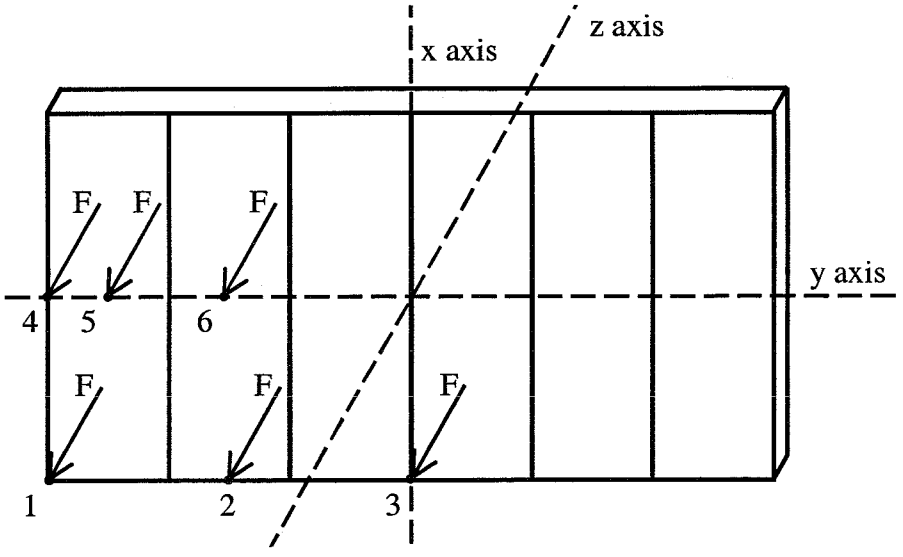

Figure 11 Load cases defined.

4.1.1 FITTING THE FEM-MODEL

The box is made out of stainless steel, the material used in the calculations is a fitted material as shown in Table 5.

Table 5 Fitted material properties.

Material property	Value
Young's modulus*[1]	165e9 [N/m^2]
Poisson's ratio	0.33 [-]
Density	7800 [kg/m^3]

*[1] With respect to the material properties it has to be mentioned that the Young's modulus has been modified to get a better fit between model and measurements, see notes below and Table 6.

Notes:

The modal FEM results differed (5%-8.6%) from the measurements. There was no observed reason for this discrepancy. As a possible solution a parameter study has been performed to find out whether dimensional and material parameters are very sensitive to variation ([Keunen, 2001]). It was seen that small parameter variations have no significant influence on the results of the modal analysis. No connection was therefore found between a dimensional or material parameter and the difference between the measurements and the FEM results. One of the remaining causes of the discrepancy is the quality of the weldings, probably resulting in non-rigid interfaces between the different plates.

The FE model has been fitted to the experiments by decreasing the E-module to 165e9 N/m2. This is a common way to "fit" a FE model to measurements. By doing this, the acoustical calculations can be compared to measurements (see next paragraph). The fitted FE model is from now on used in the analyses.

4.1.2 MODAL RESULTS

Calculating up to 180 Hz reveals about 20 modes, of which a large part show local plate deformation patterns (plate modes). To make a comparison between measurements and calculations, 3 global mode shapes are taken into account. The results are shown in Table 6, and Figure 12 - Figure 14. In the lower right corner of the figures the mode shape of the metro frame is shown.

Table 6 Modal analysis, the eigenfrequencies.

Mode shape	Measurements [Hz]	FE model			
		Real [Hz]	Error [%]	Fit [Hz]	Error [%]
Bending mode around the x-axis	95.9	102	6.4%	95.8	0.1%
Double bending mode around the x-axis	139.1	151	8.6%	147.1	5.8%
Torsion mode	159.1	167	5.0%	156.2	1.8%

In Table 6, the error values are the errors made between the measurements and the 2 (not fitted model and the fitted model) FE models. As mentioned before, the calculations are done with the fitted model. As can be seen, the error in the eigenfrequency of the fitted FE model can be neglected for the first mode. In the

second mode, the error is larger. This can have an unpleasant effect on the results later on in the project. The surrounding sound pressure is measured per frequency and in the reciprocity part used to calculate the acceleration per frequency. A shift in the eigenfrequencies can therefore result in a significant error in the accelerations due to the variation of the sound PSD per frequency. In Figure 20 the sound pressures PSD measured around the box is shown.

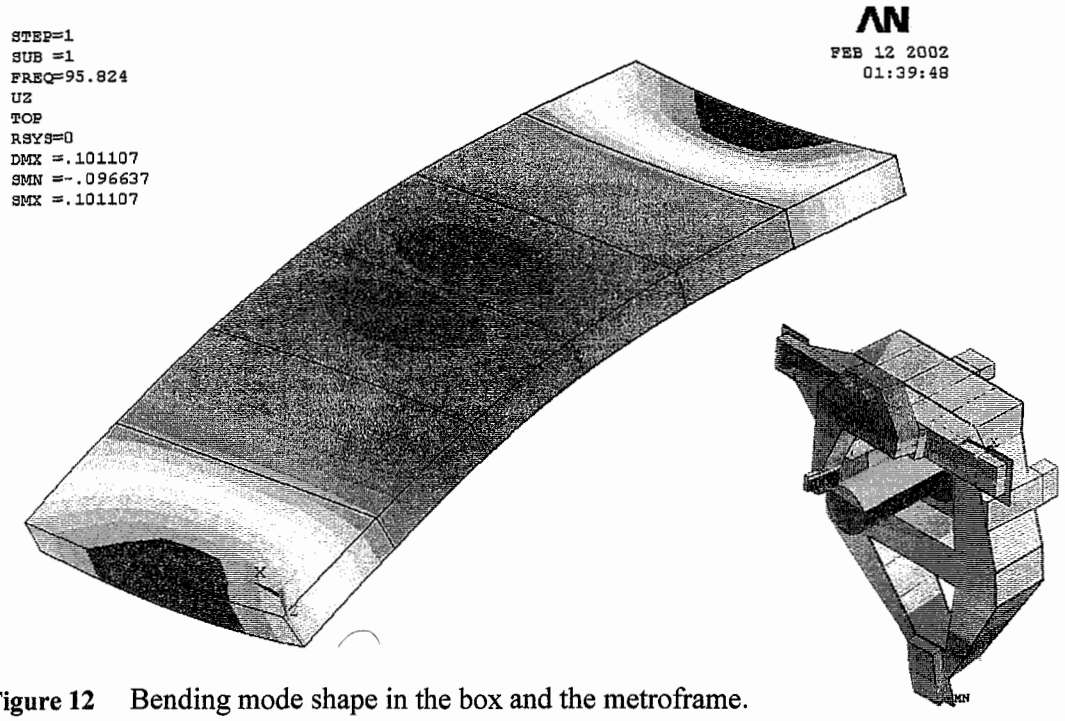

Figure 12 Bending mode shape in the box and the metroframe.

In Figure 12 a bending mode around the x-axis is shown. As can be seen, there is also a (small) bending around the y-axis.

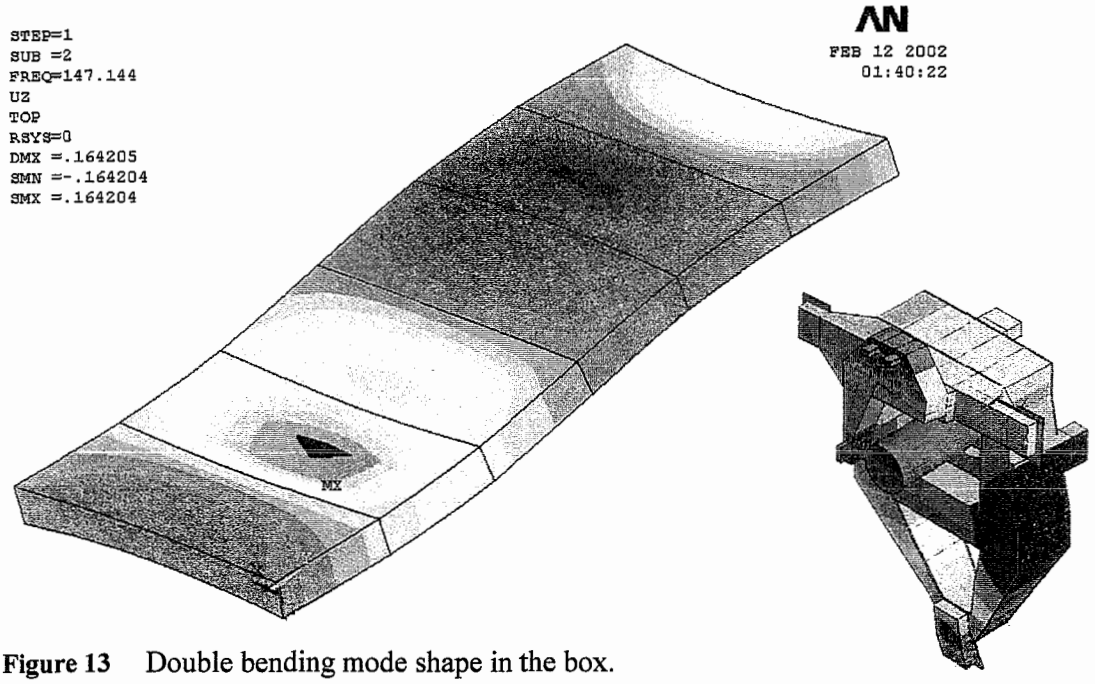

Figure 13 Double bending mode shape in the box.

Figure 13 is showing the double bending mode around the x-axis. It can clearly be seen that there are local displacements of the top-plate, between the vertical coupling plates.

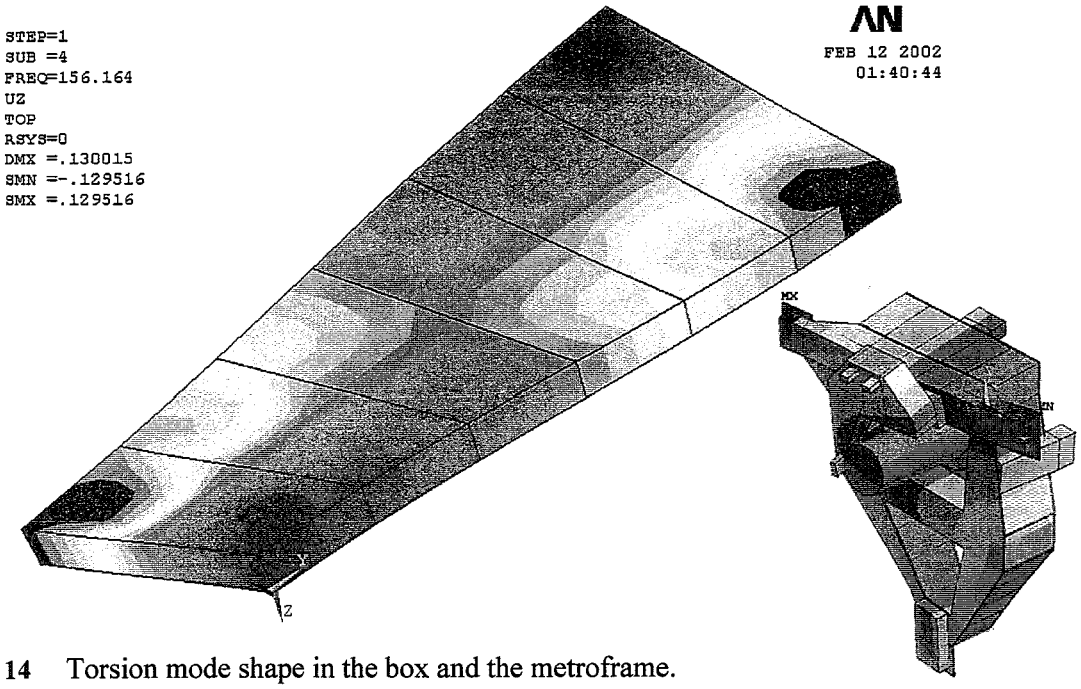

Figure 14 Torsion mode shape in the box and the metroframe.

The torsion mode is clearly visible in Figure 14 both in the metro frame and the box.

The modal results can be used to perform the harmonic calculation.

4.1.3 HARMONIC RESULTS

The harmonic modal superposition results are nodal velocity fields as a function of the frequency. As an example in Figure 15 a resulting velocity field is shown for the first eigenfrequency.

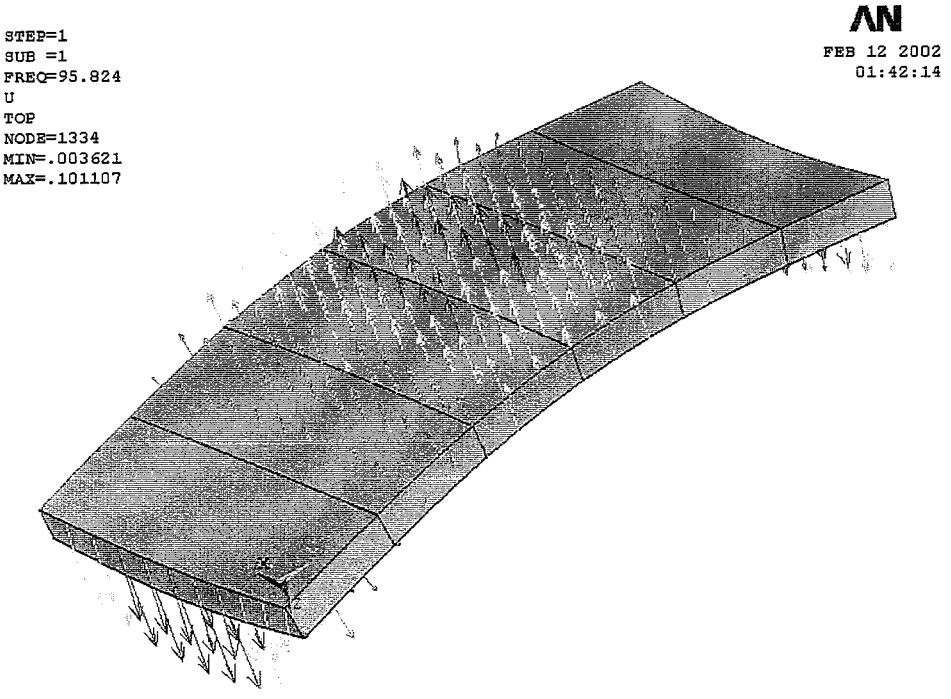

Figure 15 Nodal velocity field at 95.8 Hz.

In Figure 16 the z-displacement (of the input points) as function of the frequency is plotted for the first 3 load cases. As expected, the largest displacements occur at the eigenfrequencies, further conclusions are drawn later on.

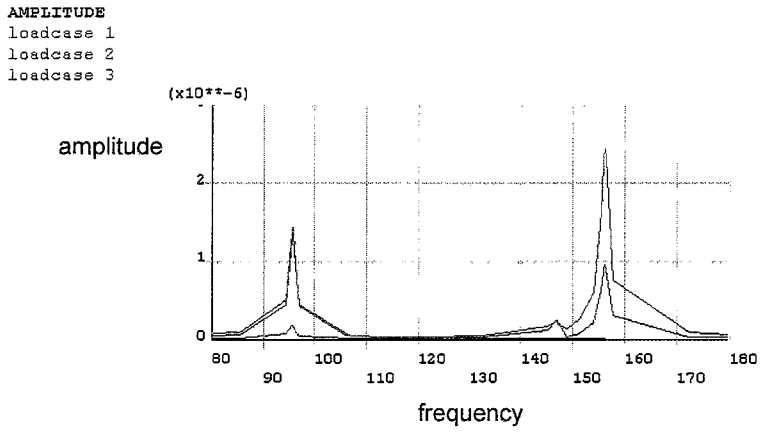

Figure 16 Displacement in z-direction of the first 3 load cases.

Note:

> The number of frequency points is not very large, as this will increase the calculation time in the acoustical step. On the other hand will it introduce an error because in the reciprocity step a linear interpolation is done between points. The error in the displacement (and therefore also in the velocity) is an overestimation of maximal a factor 2.

The results from these mechanical analyses (the calculated frequency points, not the interpolated points) are exported to NEO to perform an acoustical analysis.

4.2 ACOUSTICAL RESULTS

The acoustical results received from NEO must be viewed in Matlab, as NEO provides its post-processing functions via Matlab.

The radiated sound power calculated by NEO is shown in Figure 17. The irregular curved lines in the figure originate from the limited number of frequency points causing straight lines in Figure 16. The transformation from the straight lines to a dB scale causes curvature. As the displacements were overestimated, the radiated acoustic power is also overestimated.

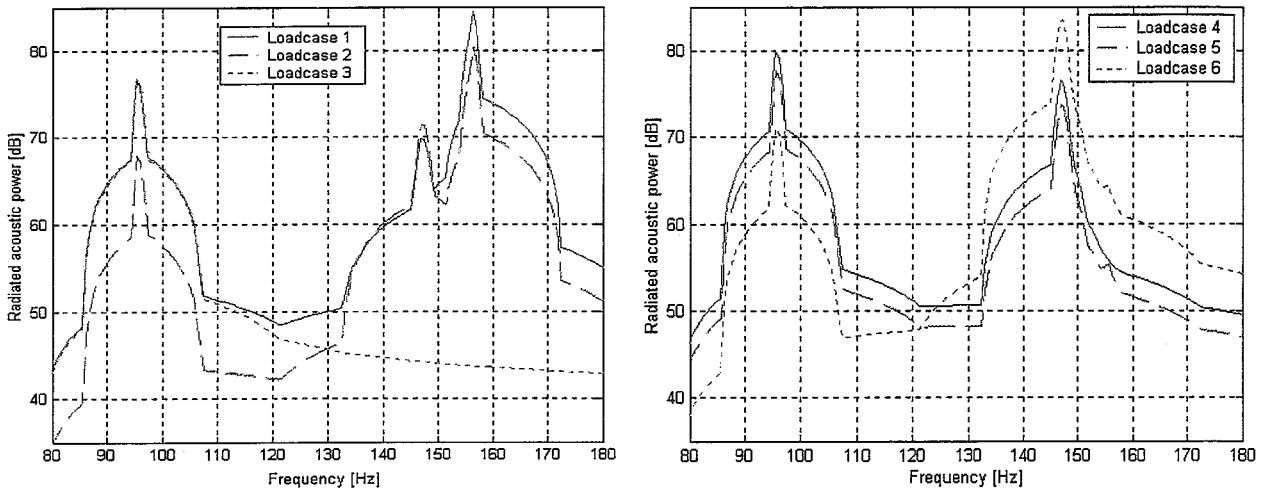

Figure 17 Radiated sound power in all 6 load cases.

From Figure 17 it can be seen that at the eigenfrequencies, the radiated sound power is high. The first peak in both graphs reveals the bending mode at 95.8 Hz and the second peak is due to the double bending at 147.1Hz. The third peak should reveal the torsion mode, but in the second graph all three load cases are located on a nodal line so it doesn't show there.

The first graph shows that load case 3 only has a peak in the bending mode. This can be explained, as the force of load case 3 is attached to the box in a nodal line of the double bending and torsion mode.

In load case 1 and 2 the torsion mode accounts for the highest radiated sound power. In load case 3, 4 and 5 the bending mode is the highest radiating mode. Load case 6 radiates the sound power most in the double bending mode.

Load case 1 and 4 are located on the same y value. Load case 4 however radiates more than load case 1 in both the bending as the double bending modes. This could be due to the (small) bending around the y-axis as seen in Figure 12.

To gain insight in the acoustical analysis, the surface pressures and the surrounding pressure fields can be examined. In Figure 18 an example of the real part of the surface pressures on the box is shown. In Figure 19 an example of the real part of the surrounding pressure field is shown at the symmetry yz-plane through the middle of the box.

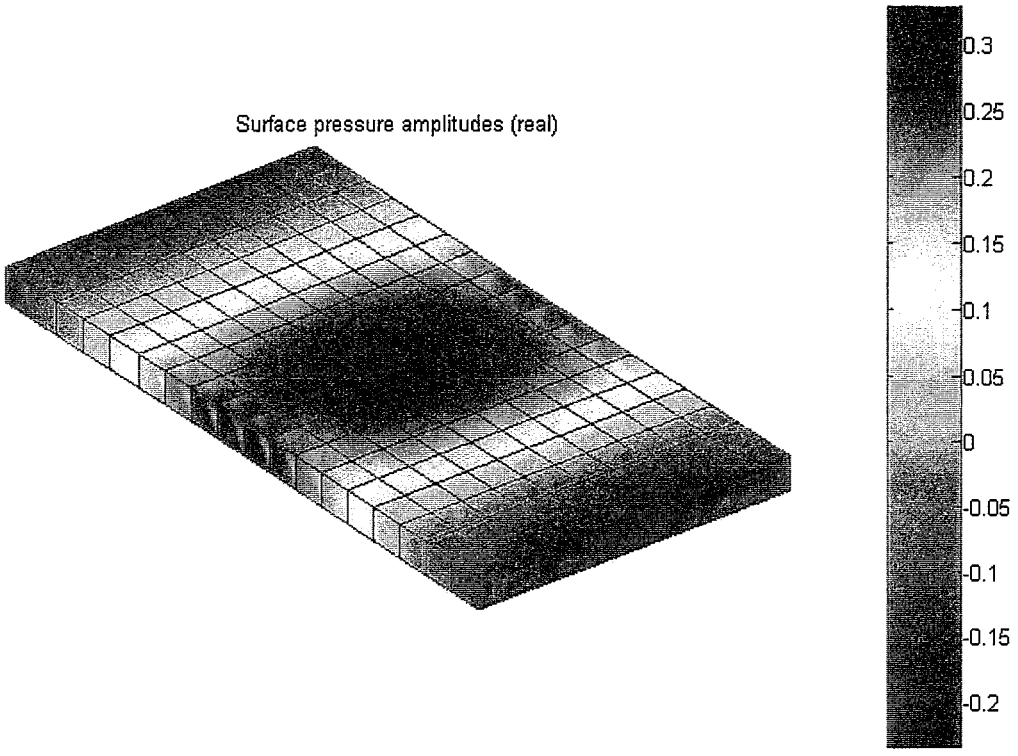

Figure 18 Real part of the surface pressures at 95.8 Hz.

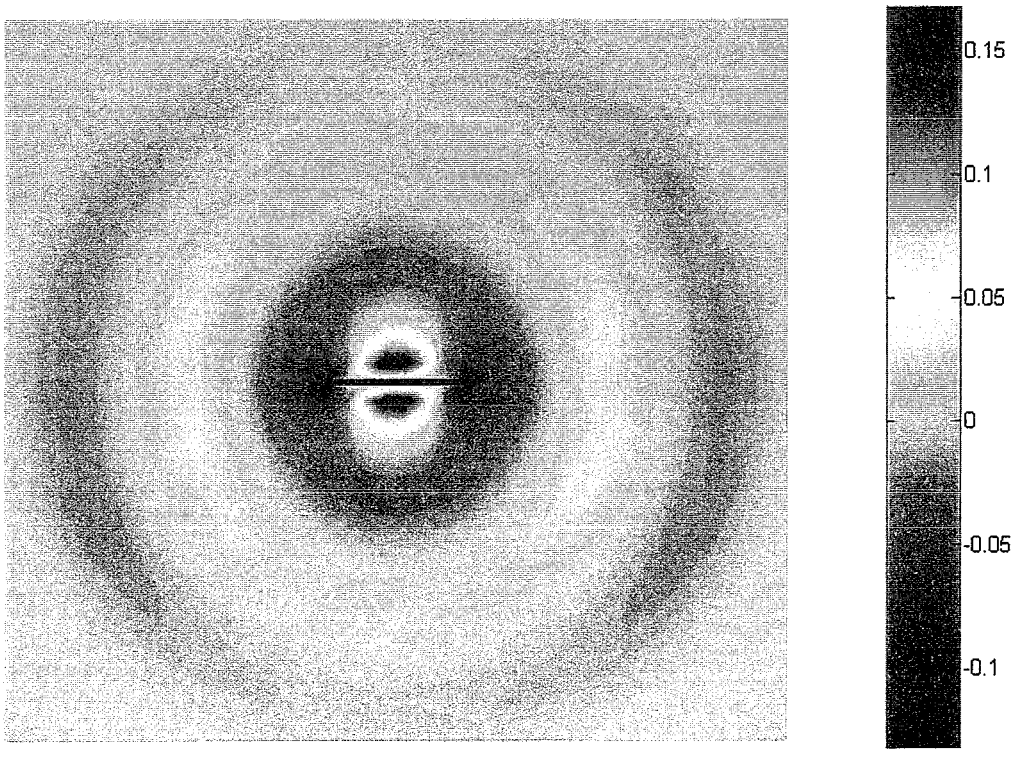

Figure 19 Real part of the surrounding pressure field at the symmetry yz-plane at 95.8 Hz.

Figure 18 shows that the surface pressures are (double) symmetric. These surface pressures look a lot like the first bending mode shape of Figure 12.

In Figure 19 can be seen that near the box, the real part of the sound pressures are high, especially in the antinode of the box (also seen in Figure 18). The sound pressure field is also a (double) symmetric field.

Note:

> In the first acoustical analyses, the results were not satisfying, as the field was not symmetric. To verify the results, a benchmark was made of a translating round disk and compared to the theory. The validation showed that the results from NEO were correct. Afterwards it showed that the velocity fields contained errors because not all the normals of the FE model were pointed outwards.

Having calculated the normalized radiated sound power; the reciprocity step can be made.

4.3 RECIPROCITY RESULTS

For the reciprocity step it is necessary to have sound pressures for the acoustical excitation of the box. They have been measured around the box leading to a sound pressure PSD as shown in Figure 20. For the details of the measurement in a reverberant room at Philips Natlab, see [Hoon, 2000].

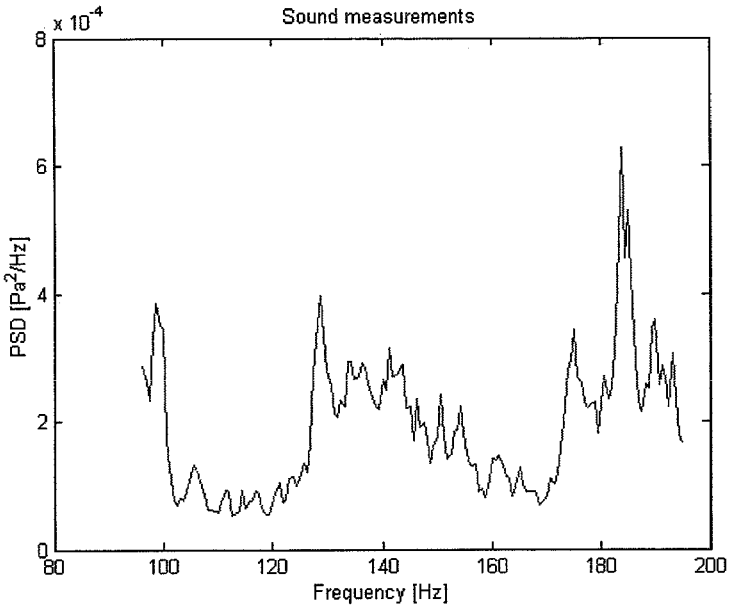

Figure 20 Sound pressure PSD measured around the box.

The importance of the correct value of the eigenfrequency can be shown with Figure 20. In the not fitted FE model, the bending mode lies at 102 Hz, instead of the measured 95.9 Hz. This would have a large influence on the results, as the measured pressures vary from 3 Pa^2/Hz at 95.9Hz to 0.8 Pa^2/Hz at 102 Hz. Fitting the model at the bending mode ensured that this didn't occur. The double bending mode at 147.1 (in stead of 139.1 Hz) Hz and the torsion mode at 156.2 Hz (in stead of 159.1 Hz) are (accidentally) less sensible to variation.

With the measured sound pressure PSD and some work in Matlab, the 3σ acceleration values are calculated according to paragraph 3.2.4. In Figure 21 the cumulative 3σ acceleration values are shown.

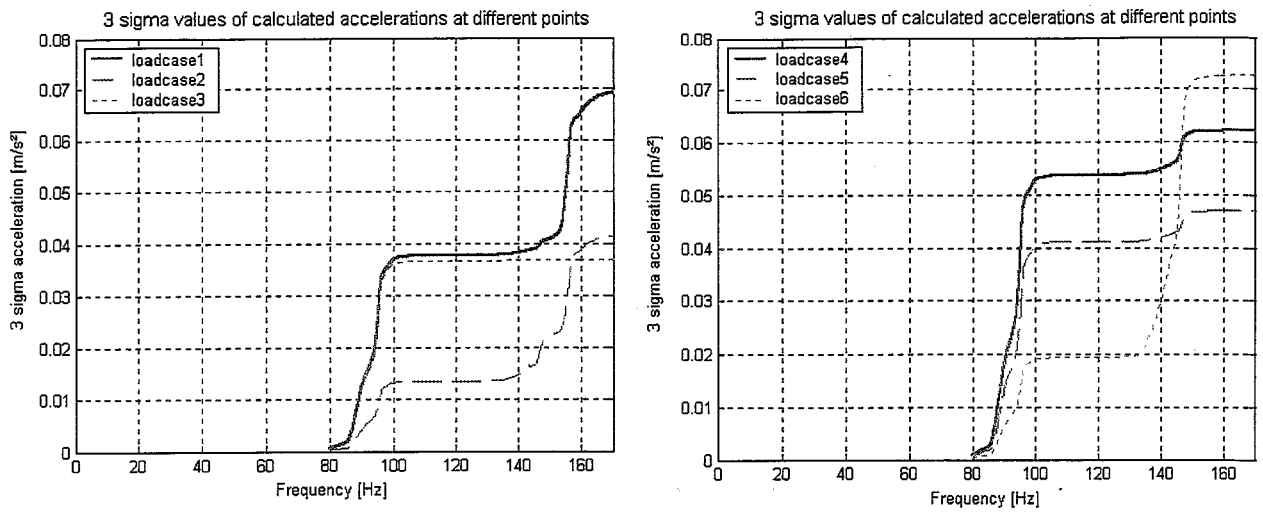

Figure 21 Cumulative 3σ z-acceleration values of all 6 load cases.

The graphs confirm that the largest part of the acceleration is due to vibrations at the resonance frequencies. This phenomenon is also confirmed by literature [Fahy, 2001].

As can be seen in Figure 21 the bending mode at 95.8 Hz gives a large contribution to the total acceleration in all 6 load cases. The lowest of these contributions are load cases 2 and 6, because these are located near the nodal line of the mode.

Looking at the double bending mode at 147.1 Hz, load case 3 is located at the nodal line of the mode. Load cases 1, 2, 4 and 5 show some increase in the acceleration. Load case 6 shows a very large increase, this is due to the local displacement of the plate as seen in Figure 13.

The torsion mode at 156.2 Hz contributes a large part in the total acceleration of load case 1 and 2. The remaining load cases have no contribution, as they all lie on a nodal line.

To check the results, they were compared to measurements done preceding this project.

4.4 VALIDATION OF THE CALCULATIONS

The results of the calculations can be validated by measurements done in a reverberant room. These measurements are described in [Hoon, 2000]. In Figure 22 and Figure 23 the measurement results are shown next to the calculations. The vertical scale of the calculation results is changed so that it matches with the measurement scale (the complete scale is seen in Figure 21).

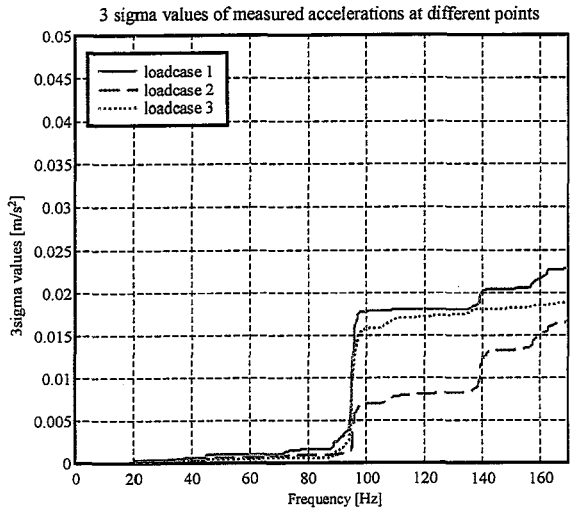

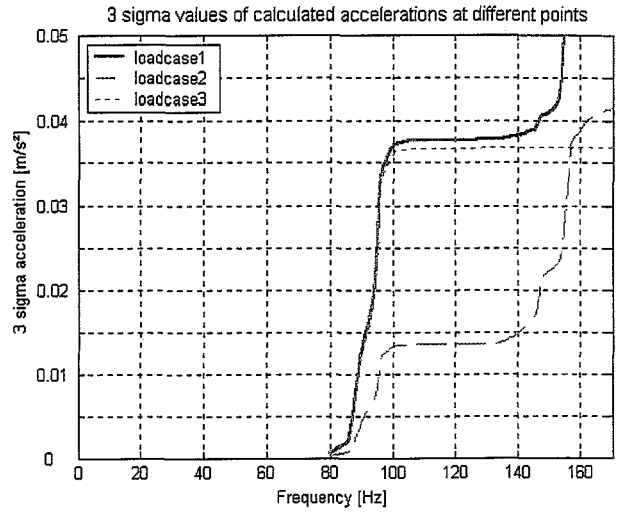

Figure 22 **a** Measurement results load case 1-3 **b** Calculation results load case 1-3

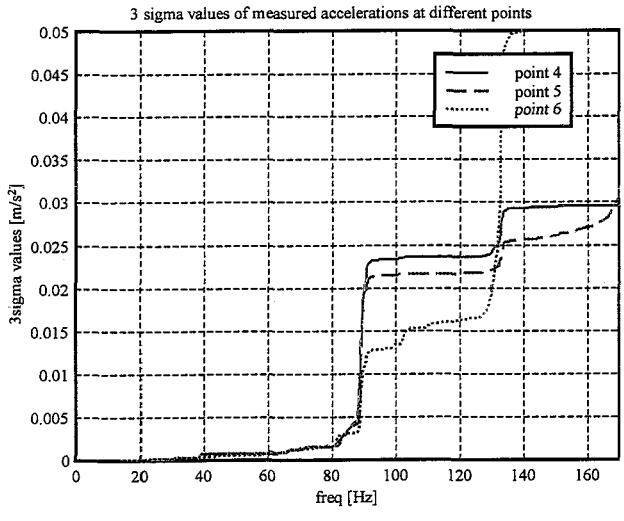

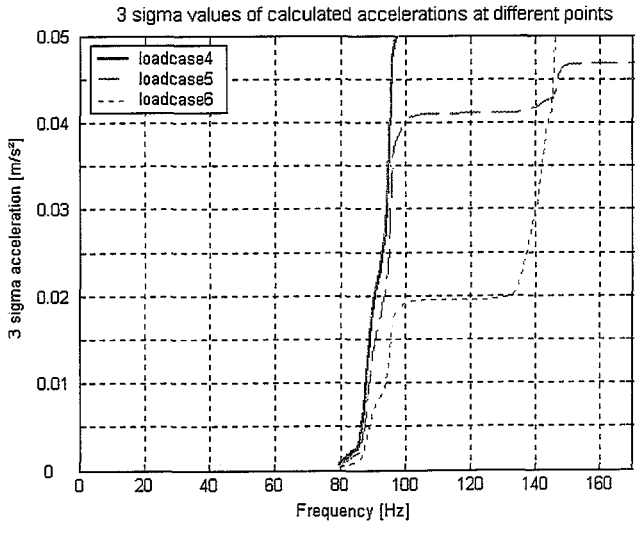

Figure 23 **a** Measurement results load case 4-6 **b** Calculation results load case 4-6

Table 7 Comparison between measurements and calculations

	Contribution bending			**Contribution double bending**		
	σ^2_{Meas}	σ^2_{Calc}	$\sqrt{\frac{\sigma^2_{Calc}}{\sigma^2_{Meas}}}$	σ^2_{Meas}	σ^2_{Calc}	$\sqrt{\frac{\sigma^2_{Calc}}{\sigma^2_{Meas}}}$
Loadcase	$[(m/s^2)^2]$	$[(m/s^2)^2]$	[-]	$[(m/s^2)^2]$	$[(m/s^2)^2]$	[-]
1	$(0.018)^2$	$(0.038)^2$	2.14	$(0.021)^2$-$(0.018)^2$	$(0.041)^2$-$(0.038)^2$	1.38
2	$(0.007)^2$	$(0.014)^2$	2.00	$(0.013)^2$-$(0.007)^2$	$(0.023)^2$-$(0.014)^2$	1.67
3	$(0.016)^2$	$(0.037)^2$	2.31			
4	$(0.022)^2$	$(0.053)^2$	2.41	$(0.029)^2$-$(0.022)^2$	$(0.062)^2$-$(0.053)^2$	1.70
5	$(0.020)^2$	$(0.042)^2$	2.10	$(0.026)^2$-$(0.020)^2$	$(0.046)^2$-$(0.042)^2$	1.13
6	$(0.011)^2$	$(0.021)^2$	1.91	$(0.050)^2$-$(0.011)^2$	$(0.072)^2$-$(0.021)^2$	1.41
		mean	2.15		**mean**	1.46
		st.dev.	0.19		**st.dev.**	0.23

Notes:

The measured and calculated values seen in Table 7 are derived from Figure 22 and Figure 23.

Some cells in Table 7 are left blank, as the load of that load case lies on a nodal line and no contribution to the acceleration is found.

As seen in Table 7, the overall error made in the bending mode is a factor 2.15 with a standard deviation of 0.19. The double bending mode differs a factor 1.46 with a standard deviation of 0.23. For the torsion mode only 2 load cases were available and the errors found are rather high. Therefore no conclusions will be drawn from these load cases.

The errors found can partly be explained by the small number of frequency points (see Figure 16 and Figure 17). The cumulative nature of the results will add to these errors.

The calculations performed in [Hoon, 2000] showed about a factor 2 between the measurements and the calculations.

CHAPTER 5

CONCLUSIONS AND RECOMMENDATIONS

5.1 CONCLUSIONS

Overall it can be concluded that excitation due to a diffuse sound field can be calculated with the procedure developed in this project. The error factors found between the measurements and the calculations are fairly low.

Some overall conclusions can be drawn:

- The error made between measurements and calculations of the contribution of the bending mode to the acceleration is around a factor 2. This factor does not vary a lot (standard deviation of 0.19) through the different load cases.
- The contribution of the double bending mode to the acceleration is predicted almost correct (< factor 1.7), with a standard deviation through the load cases of 0.34.
- No conclusions can be drawn for the torsion modes, as only 2 results are available with a large error and standard deviation.
- Because the used box is dynamically and geometrically rather similar to the construction of the metroframe, it is expected that the response of a metroframe in a diffuse field can also be predicted with the same accuracy.
- The small number of frequency points can partly explain of the errors found, as an overestimation is made due to linear interpolation. More frequency points will solve this problem, but it will also increase the calculation time considerably.
- As the procedure takes a lot of steps there must be a decent administration to keep track of the parameters, files and results.
- 3 different software tools were used; Ansys, NEO and Matlab, each with its own user interface, interpretation and definitions. Therefore the procedure does not run automatically.

5.1.1 ANSYS CONCLUSIONS

- Multiple load cases in a mode superposition analysis are not possible without some programming. Simple filling of the matrices is not possible, as the number of nodes and frequency steps use up the available memory.
- Clustering around eigenfrequencies is useful to decrease the number of frequency steps and keep the accuracy needed. But in the mode superposition steps problems arise that are not solved yet.
- It is not recommended solving the modal superposition analysis in Matlab. All nodes on the surface must be taken into account, resulting in even for Matlab computational matrices. In Ansys there are dedicated solvers to solve large matrices.

5.1.2 NEO CONCLUSIONS

- Solving the acoustical problems takes quite a while, as the full matrices must be calculated and a fine mesh is used. Every frequency step takes disc space for the results, resulting in a lot of used space at the end of an analysis.
- The post-processing of NEO is performed in Matlab. This demands some knowledge of Matlab as the routines have some hidden options in the sources.
- The benchmark solved in NEO produced results in agreement with to the theory.

5.2 RECOMMENDATIONS

- More calculations must be done with this procedure preferably on a different model to find out how accurate and robust it is.
- Calculations must be done with bigger hardware to make it possible to use a lot of frequency steps in a large range.
- The metro frame must be analysed with this procedure. This is also a way of validating the procedure as measurements were already done.
- Parameter studies must be done to be able to examine the influence of the sound field on different constructions.
- As NEO has no graphical user interface, the communication is sometimes not clear. A user interface will increase the user friendliness.
- There should be a way of changing the element size between the FEM and the BEM analysis. A larger element size in BEM results in less elements, directly resulting is less solving time.
- As the present procedure only works with a diffuse sound field, the procedure must be extended to be able to calculated sound induced vibration for all kinds of sound fields.
- When using Matlab as a base platform from where the FEM tool en the BEM tool can be started and evaluated, an optimisation tool can be used in a closed loop optimisation analysis. This is a complementary step that can only be taken if the procedure is accurate and robust.

BIBLIOGRAPHY

1. [Keunen, 2001] Harm Keunen, *Sound radiation of a box shaped mode, a literature study*, 2001
2. [Verheij, 1997] Prof.dr.ir. J.W.Verheij, *International Journal of Acoustics and Vibration*, Volume 2, Number 3, page 103, September 1997
3. [Verheij, 1996] Prof.dr.ir. J.W.Verheij, *Basiskennis geluidarm construeren*, Syllabus
4. [Verheij, 1994] Prof.dr.ir. J.W.Verheij, *ANTEASR-Handbook on procedures for sound path quantification*
5. [Ansys, 2002] Ansys Inc., *ANSYS 6.0 Documentation*, 2001
6. [Hoon, 2000] Corne De Hoon, *PIR Modeling of Sound structure interaction*, ASML report, 2000
7. [Gompel, 2000] Dirk Van Gompel, *TAR Acoustical measurements clean rooms Taiwan*, ASML report, 2000
8. [TNO, 2000] TNO, *Resultaat fase 1 geluidsonderzoek clear air system*, ASML report, 2000
9. [Fahy, 1985] Frank J. Fahy, *Sound and structural vibration*, 4th print, London: Academic Press, 1994, ISBN/ISSN 0-12-247671-9 . - 0-12-247670-0
10. [Fahy, 1990] Frank J. Fahy, John G. Walker, *Fundamentals of noise and vibration*, London : Spon, 1998, ISBN/ISSN 0-419-24180-9 . - 0-419-22700-8
11. [Fahy, 2001] Frank J. Fahy, *Foundations of engineering acoustics*, London : Academic Press, 2001, ISBN/ISSN 0-1224-7665-4
12. [Kinsler, 1982] Lawrence E. Kinsler, Austin R. Frey, Alan B. Coppens, *Fundamentals of acoustics*, 4th ed., Chichester : Wiley, 2000, ISBN/ISSN 0-471-84789-5
13. [Kuijpers, 1999] Ard H.W.M. Kuijpers, *Acoustic modeling and design of MRI scanners*, doctoral thesis, Eindhoven : Technische Universiteit Eindhoven, 1999, ISBN/ISSN 90-386-0648-6
14. [Kessels, 2001] Peter H.L. Kessels, *Engineering toolbox for structural-acoustic design : applied to MRI-scanners*, doctoral thesis, Eindhoven : Technische Universiteit Eindhoven, 2001, ISBN/ISSN 90-386-2682-7
15. [Bathe, 1982] Klaus-Juergen Bathe, *Finite element procedures in engineering analysis*, Englewood Cliffs : Prentice-Hall, 1982, ISBN/ISSN 0-13-317305-4
16. [BEM] BEM for engineers, ASML report
17. [NEO, 2001] NEO manual, http://www.dolfyn.com

APPENDIX A

Diffuse field

The ideal probabilistic model, which is universally adopted to deal with the problem of describing and quantifying sound fields in reverberant enclosures, is that of the diffuse field. The central concept is that of a sound field consisting of a very large set of statistically unrelated (uncorrelated) elemental plane waves of which the propagation direction is random with a uniform probability distribution. [Fahy, 2001]

In an enclosure where the walls reflect sounds the total sound field consists not only of direct sound pressures, but also of indirect sound pressures (see Figure 24).

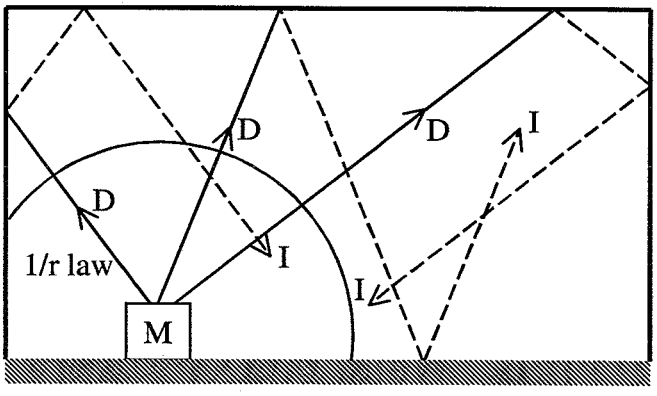

Figure 24 Machine in a reverberant room with reflecting walls.
M=Machine, D=Direct sound, I=Indirect sound

When an observer is close to the machine the 1/r law for a point monopole source applies as the direct sounds dominates. When the observer is farther away, indirect sounds are added to the direct sounds. In this region, the sound pressure levels are nearly constant with the distance to the machine. The sound field generated in this region is called a diffuse field.

Some properties of a diffuse field that are used in this project will now be discussed (see [Verheij, 1996] page 5-08).

The energy balance of a diffuse field can be written as.

Equation 27 $$P_{rad} = V_{room} \cdot \frac{dE'}{dt} + 2 \cdot \delta \cdot V_{room} \cdot E'$$

where:

P_{rad} = Sound power.

$V_{room} \cdot \frac{dE'}{dt}$ = Energy increase in the room.

$2 \cdot \delta \cdot V_{room} \cdot E'$ = Energy dissipation by unit of time, where the energy density $E' = \frac{\overline{p_{rev}^2}}{\rho c^2}$.

Equation 27 can be rewritten with for $\delta = \frac{6.9}{T_{60}}$ and assuming stationary state, $\frac{dE'}{dt} = 0$

Equation 28 $$P_{rad} \approx \frac{13.8}{T_{60}} \cdot \frac{\overline{p_{rev}^2}}{\rho \cdot c^2} \cdot V_{room} \approx \overline{p_{rev}^2} \cdot \frac{13.8 \cdot V_{room}}{\rho \cdot c^2 \cdot T_{60}}$$

In this equation, T_{60} is the reverberation time of the room. It is the time it takes for the sound level to fall off 60 dB after the sound source is switched off. This is directly linked to what extend the walls will absorb the reflecting sounds.

The Sabine law states that the reverberation time is linked to the room's volume V_{room} by the equivalent absorbing surface A.

Equation 29 $$T_{60} \approx \frac{55.2}{c} \frac{V_{room}}{A}$$

Substituting Equation 29 into Equation 28 leads to the power equation used in this project for the reciprocal experiment.

Equation 30 $$P_{rad} = \overline{p_{rev}^2} \cdot \frac{A}{4 \cdot \rho \cdot c}$$

Increasing the equivalent absorbing surface A (less sound absorption in the wall) thus increases the sound power in the room with a constant source.

APPENDIX B

Mechanical analysis

The mechanical (FEM) analysis consists of 2 parts; the modal analysis and the harmonic response analysis using modal superposition (see [Ansys, 2002]).

B.1 Modal analysis

The eigenvalue and eigenvector problem needs to be solved for a modal analysis. It has the form of:

Equation 31 $$[K]\{\phi_i\}=\lambda_i[M]\{\phi_i\}$$

where:

$[K]$ = Structural stiffness matrix.

$\{\phi_i\}$ = Eigenvector.

λ_i = Eigenvalue.

$[M]$ = Structural mass matrix.

The eigenvalue and eigenvector extraction procedures available in Ansys include the reduced, subspace, block Lanczos, damping, a.o. Each method has its own usage and extraction technique. In this analysis the block Lanczos method is used as it is optimized for large symmetric eigenvalue problems and no damping is present. Typically, this solver is applicable to the type of problems solved using the subspace eigenvalue method, however, at a faster convergence rate.

The subspace iteration method is described in detail by [Bathe, 1982].

After the modal analysis the eigenvalues and eigenvectors are written to the results file. When it is desirable to review mode shapes in the post-processor, a modal expansion pass is needed. In an expansion pass the mode shapes are written to the results file.

B.2 Harmonic response with modal superposition

Mode superposition method is a method of using the natural frequencies and mode shapes from the modal analysis to characterize the dynamical response of a structure to steady harmonic excitations.

The equations of motion may be expressed as:

Equation 32 $$[M]\{\ddot{u}\}+[C]\{\dot{u}\}+[K]\{u\}=\{F\}$$

where:

$\{F\}$ = Time-varying load vector, given by:

Equation 33 $$\{F\}=\{F^{nd}\}+s\cdot\{F^{s}\}$$

where:

$\{F^{nd}\}$ = Time varying nodal forces.

s = Load vector scale factor (input on the LVSCALE command).

$\{F^{s}\}$ = Load vector from the modal analysis.

The load vector $\{F^{s}\}$ is computed when doing a modal analysis with forces applied. The time varying nodal force $\{F^{nd}\}$ can be applied after the modal analysis. This makes it possible to make several mode superposition analyses succeeding one modal analysis.

[Bathe, 1982] developed a way to adapt Equation 32 to an equation of motion in modal coordinates y_j. First a set of modal coordinates y_i is defined such that

Equation 34 $$\{u\} = \sum_{i=1}^{n} \{\phi_i\} \cdot y_i$$

where:

$\{\phi_i\}$ = Mode shape of mode i.

n = Number of modes to be used (input as MAXMODE on the HROPT command).

Substituting Equation 34 into Equation 32, subsequently rewriting and solving results in an equation of motion in modal coordinates.

Equation 35 $$\ddot{y}_j + 2\omega_j \xi_j \dot{y}_j + \omega_j^2 y_j = \{\phi_j\}^T \{F\}$$

where:

ξ_j = Modal damping for mode j (see appendix B.4).

ω_j = Natural circular frequency of mode j.

Since j represents any mode, Equation 35 represents n uncoupled equations in the n unknown y_j. The advantage of the uncoupled system is that all the computationally expensive matrix algebra has been done in the eigensolver. Therefore long transients may be analyzed inexpensively in modal coordinates. In harmonic analysis frequencies may be scanned faster than by a reduced harmonic response method.

B.3 Expansion pass

The expansion pass starts with the reduced harmonic response solution in modal coordinates and calculates the complete displacement, stress, and force solution at all degrees of freedom. These calculations are done at all the specified frequency steps.

The y_j are converted back into geometric displacements $\{u\}$ (the system response to the loading) by using Equation 34. That is, the individual modal responses y_j are superimposed to obtain the actual response, and hence the name "mode superposition".

This step is needed to be able to export the nodal velocity field per frequency step to NEO.

B.4 Modal Damping

The modal damping ξ_j, is the combination of several Ansys damping inputs:

Equation 36 $$\xi_j = \frac{\alpha}{2\omega_j} + \frac{\beta\omega_j}{2} + \xi + \xi_{mj}$$

where:

α = Uniform mass damping multiplier.

β = Uniform stiffness damping multiplier.

ξ = Constant damping ratio (input on the DMPRAT command).

ξ_{mj} = Modal damping ratio (input on the MDAMP command).

In the mode superposition method using Lanczos and subspace extraction methods, only Rayleigh or constant damping is allowed so that explicit damping is not allowed by the mode superposition procedure.

APPENDIX C

What is 'POWER SPECTRAL DENSITY'?

by Dr Peter Spence

Many analysts who make the transition from static to dynamic analysis find themselves baffled by the peculiar concept of power spectral density. It seems to raise almost as many questions as it answers, e.g. why (acceleration)^2, why not just acceleration, what has power to do with anything, etc, etc. Who remembers some of those deathless definitions like "the p.s.d. is the Fourier Transform of the auto-correlation function..."? Well, here is a laymans guide to the meaning of life, the universe and power spectral density.

We need to begin with the origins of investigations into random signals. Electronics engineers were interested in trying to characterise noise in their equipment in the late 1940's. Remember that all equipment used valves then and the oldies amongst us will recall the interesting hums and buzzes you used to hear when tuning radios.

A typical time-history of noise consisted of a randomly varying signal such as indicated in Figure 1. Note that both the amplitude and the frequency of short sections of the signal have random variations. There is no way of using previous data to precisely predict future sections of the signal.

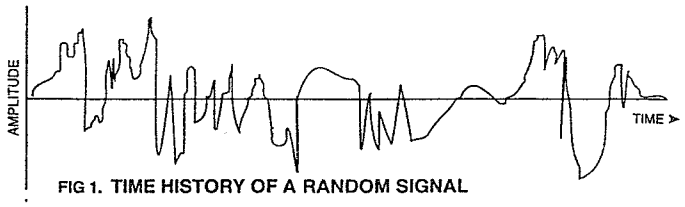

FIG 1. TIME HISTORY OF A RANDOM SIGNAL

PSD

It was evident that one could use some sort of peak amplitude to describe the signal but that was not very helpful so a method of analysis based on statistical methods was devised. We note that over a relatively long time the signal has average amplitude of zero. However, in the same way that the statisticians can calculate the standard deviation in a sample of random varying measurements, e.g. weight of bags of crisps, then it must also be possible to determine a similar parameter for a continuously varying signal. The mathematics is fairly straightforward but the method of actually doing it involved using techniques from analogue computers (remember those?)

By passing the signal through a multiplying circuit, so that it was multiplied by itself, one then obtain (amplitude)^2. This has the obvious characteristic (Figure 2) that, whereas the original signal had positive and negative values, the squared signal is entirely positive. Now we can pass the signal through a filter and obtain an average value. This is known as the mean square value.

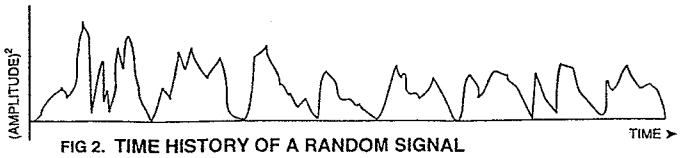

FIG 2. TIME HISTORY OF A RANDOM SIGNAL MULTIPLIED BY ITSELF

By using another circuit to generate the square root of the mean square value we arrive at the root mean square, or rms, value of the signal. This is no different from the standard deviation in a statistical analysis.

Now, the rms is a useful parameter as it enables one to compare the overall intensity of two random signals. However it does not give any information regarding the frequency content.

To determine this the (amplitude)^2 signal is passed through a low-pass filter. This is a device that allows all components of the signal with a frequency less than the cut-off frequency for the filter to pass through it. High frequency components are filtered out as indicated in Figure 3.

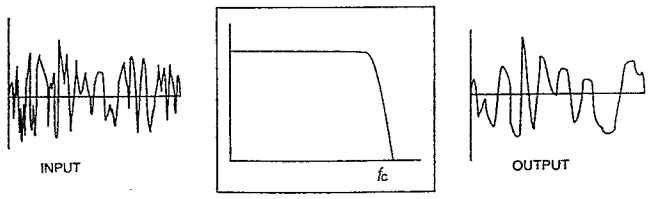

FIG 3.

If one then plots the mean square value for the filtered signal as a function of the cut-off frequency a result similar to that shown in Figure 4 will be obtained. Clearly, as the cut-off frequency approaches infinity the curve will tend towards the mean square value for the whole signal, known as overall mean

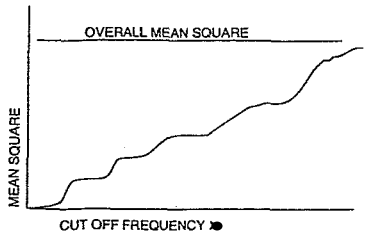

FIG 4. MEAN SQUARE Vs LOW PASS FILTER CUT-OFF FREQUENCY

square, because eventually the filter will allow the whole of the original signal to pass through.

At intermediate frequencies the curve shows sudden jumps - this is an indication that there is a significant contribution to the signal at these frequencies. So, by calculating the slope of the curve in Figure 4 the density of the mean square value with respect to frequency is obtained (Figure 5). A variation of any property with respect to frequency is referred to in terms of a 'spectrum' (from the rainbow which is a visible manifestation of the variation of frequency in the colours of visible light) which leads to the term 'Spectral Density'.

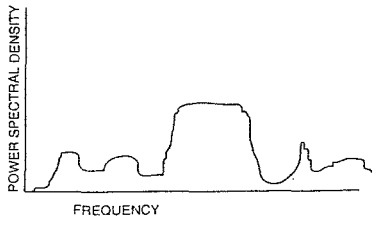

FIG 5. POWER SPECTRAL DENSITY

So much for the physical interpretation - where does the familiar "acceleration power spectral density"come from.

Remember that this method was developed by electronics engineers for whom electrical power is a key parameter. For them it is not of great importance whether power is determined as (volts x amps, $(volts)^2$ or $(amps)^2$ since Ohms Law relates volts and amps through resistance. Thus dynamicists have adopted the concept of $(acceleration)^2$ as the unit to define random vibration.

Hence acceleration power spectral density is a measure of the power in random vibration (measured as acceleration) as a function of frequency. It is evident that one could have plotted rms values versus frequency in figure 4 and then obtained a spectral density in acceleration/Hz units but nobody does!

The cumbersome procedure described above was the basis of analogue methods of analysing random vibration for many years. With the arrival of the Fast Fourier Transform (FFT) and digital computers the analysis of vibration signals was made infinitely easier. Now you can sit in front of a CRT display and watch PSD displays being generated faster than the data can be captured. In fact, it could be argued that the FFT is one of the most significant new tools for engineering analysis in the second half of this century.

The fact that we now have methods to easily measure and characterise random vibration means that it now features very strongly in structural analysis and vibration testing. There is a particular type of noise or vibration known as white noise in which the p.s.d is constant, i.e. there is an equal amount of power at all frequencies. This is often encountered (in an appr imate form) in offices and bulidings as the general background noise and slight hissing from air-conditioning, computers, conversation, etc.

More particularly, random vibration is a significant problem for satellites (vibration during launch is particularly severe), military vehicles charging across rough terrain and noise-induced vibration from jet engine exhaust (for example Concorde's tail-cone during take-off).

As a rough guide to the levels of vibration, imagine sitting on a vibration machine. A p.s.d. of 0.001 g^2/Hz over 25 to 250 Hz would be similar to that experienced inside a civil airliner. If we increased the p.s.d. to 0.01 g^2/Hz we would be at a level where most electronic equipment is tested. At 0.1 g^2/ Hz we would feel quite uncomfortable, but it is typical of military vehicles and qualification test levels for satellite equipment. Going up to 1.0 g^2/Hz would certainly bring tears to your eyes!